ASAR lncRNAs control DNA replication timing through interactions with multiple hnRNP/RNA binding proteins.

Mathew J. Thayer[1,*,#], Michael B. Heskett[2,4,#], Leslie G. Smith[1], Paul T. Spellman[2,3], and Phillip A. Yates[1].

[1]Department of Chemical Physiology and Biochemistry
[2] Department of Molecular and Medical Genetics
[3]Cancer Early Detection Advanced Research Center, Knight Cancer Institute
Oregon Health & Science University
3181 S. W. Sam Jackson Park Road
Portland, Oregon 97239, USA
[4]Stanford Cancer Institute
291 Campus Drive, Stanford CA, 94305.

***Corresponding author.**

ORCID: 0000-0001-6483-1661

TEL: (503) 494-2447

FAX: (503) 494-7368

Email:thayerm@ohsu.edu

[#]These two authors contributed equally.

Abstract

ASARs are a family of very-long noncoding RNAs that control replication timing on individual human autosomes, and are essential for chromosome stability. The eight known ASAR genes express RNAs that remain closely associated with their parent chromosomes. Analysis of RNA-protein interaction data (from ENCODE) revealed numerous RBPs with significant interactions with multiple ASAR RNAs, with several hnRNPs as abundant interactors. An ~7kb domain within the ASAR6-141 RNA shows a striking density of RBP interaction sites. Genetic deletion and ectopic integration assays indicate that this ~7kb RNA binding protein domain contains functional sequences for controlling replication timing of entire chromosomes in *cis*. shRNA-mediated depletion of HNRNPA1, HNRNPC, HNRNPL, HNRNPM, HNRNPU, and HNRNPUL1 results in dissociation of ASAR RNAs from their chromosome territories, and disrupts the synchronous replication that occurs on all autosome pairs, recapitulating the effect of individual ASAR gene knockouts on a genome-wide scale. Our results further demonstrate the role that ASARs play during the temporal order of genome-wide replication, and that ASARs function as essential RNA scaffolds for the assembly of hnRNP complexes that help maintain the structural integrity of each mammalian chromosome.

42 **Introduction:**

43 The vast majority of mammalian DNA replicates in homologous regions of
44 chromosome pairs in a highly synchronous manner [1-3]. However, genetic disruption of
45 non-protein coding ASAR ("ASynchronous replication and Autosomal RNA") genes
46 causes a delay in replication timing on individual human chromosomes in *cis*, resulting in
47 highly asynchronous replication between pairs of autosomes [4-7]. There are eight
48 genetically validated ASAR genes located on human chromosomes 1, 6, 8, 9 and 15 [4-7].
49 All of the known ASAR genes share several distinctive characteristics, including: 1)
50 contiguously transcribed regions of >180 kb, 2) epigenetically regulated Allelic Expression
51 Imbalance (AEI; including mono-allelic expression); 3) Variable Epigenetic Replication
52 Timing (VERT; including asynchronous replication timing); 4) high density of LINE1 (L1)
53 sequences (>30%); and 5) retention of the RNA within their parent chromosome territory.
54 Recently, we used these notable characteristics to identify ASAR gene candidates on
55 every human autosome [5,6].

56 In addition to genetic disruption assays, ectopic integration of ASAR transgenes into
57 mouse chromosomes has been used as a second functional assay to help define the
58 critical sequences within ASAR genes that control chromosome-wide replication timing
59 [8,9]. For example, ASAR6 RNA expressed from transgenes, ranging in size from an ~180
60 kb BAC transgene to PCR products (as small as ~3 kb) containing the critical sequences,
61 remain associated with the chromosome territories where they are transcribed [8,9]. These
62 same transgenes cause delayed replication timing (DRT) and delayed mitotic
63 condensation (DMC) of entire chromosomes in *cis* [8,9]. Furthermore, ASAR6 RNA was
64 found to control chromosome-wide replication timing using oligonucleotide mediated RNA

65 degradation of ASAR6 RNA that was expressed from a BAC transgene integrated into
66 mouse chromosome 3 [9]. These findings suggest that ASARs represent ubiquitous,
67 essential, *cis*-acting elements that control mammalian chromosome replication timing via
68 expression of chromosome associated RNAs. In this report, we identify RNA binding
69 proteins (RBPs) that are critical for ASAR RNA localization and function.

70 Chromosome-associated long non-coding RNAs are known to be important for
71 numerous aspects of chromosome dynamics in diverse eukaryotes from yeast to
72 mammals [10-14]. The mammalian nucleus is rich in heterogenous nuclear RNA (hnRNA),
73 which represents >95% of the total RNA Polymerase II output [12,15]. The vast majority of
74 hnRNA is poorly defined, has been referred to as the "Dark Matter" of the genome [15], and
75 includes spliced and unspliced intronic sequences, circular RNAs [16], very long intergenic
76 non-coding RNAs [vlincRNAs; [17]], as well as poorly defined RNAs that include chromatin
77 associated RNAs [caRNAs; [18]] and repeat rich RNAs [repRNAs [19]] that can be detected
78 by C0T-1 DNA [which is comprised primarily of LINE and SINE repetitive sequences;
79 [13,20,21]]. Some of these nuclear RNAs comprise abundant species, yet lack clearly defined
80 functions, while others are thought to be the by-products of other nuclear processes and
81 have been collectively called "RNA debris" [12]. The relationship between ASAR RNAs and
82 these other chromosome-associated RNAs remains poorly defined.

83 Previous studies have suggested that long nascent transcripts that are detected by
84 C0T-1 DNA play a dynamic structural role that promotes the open architecture of active
85 chromosome territories [13,20]. The RNA species detected by C0T-1 DNA are predominantly
86 L1 sequences, and these L1 RNAs remain associated with the chromosome territories
87 where they are transcribed [20]. A link between C0T-1 RNA and ASAR RNAs is suggested

88 by the observation that ASAR RNAs contain a high L1 content and remain associated
89 with their parent chromosome territories [4-7,9]. In addition, deletion and ectopic integration
90 assays demonstrated that the critical sequences for controlling chromosome-wide
91 replication timing within *ASAR6* and *ASAR15* map to the antisense strand of L1
92 sequences located within the ASAR6 and ASAR15 RNAs [9]. In this report we found that
93 human C0T-1 DNA can detect the chromosome territory localization of ASAR6 RNA that
94 is expressed from a BAC transgene integrated into a mouse chromosome, indicating that
95 at least some of the RNA species detected by C0T-1 DNA represents ASAR RNA.

96 Heterogeneous nuclear ribonucleoproteins (hnRNPs) represent a large family of
97 abundant RBPs that contribute to multiple aspects of nucleic acid metabolism. Many of
98 the proteins that are in hnRNP complexes share general features, but differ in domain
99 composition and functional properties [reviewed in [22]]. The functions of hnRNPs vary
100 according to their subcellular localization. Most of the hnRNPs possess conventional
101 nuclear localization signals and are predominantly present in the nucleus during steady
102 state, where they function in various RNA metabolic processes including transcription,
103 splicing, export, and 3' end processing [22,23], and more recently have been implicated in
104 DNA replication [24]. A direct connection between chromosome territory associated C0T-1
105 RNA and hnRNPs was established by the observation that siRNA mediated depletion, or
106 forced expression of dominant interfering mutants, of HNRNPU results in dissociation of
107 C0T-1 RNA from chromosome territories [13,20,21]. In addition, recent studies have proposed
108 that abundant nuclear proteins such as HNRNPU nonspecifically interact with "RNA
109 debris" that creates a dynamic nuclear mesh that regulates interphase chromatin
110 structure [12,18]. Here, we used publicly available enhanced Cross Link Immuno-

111 Precipitation (eCLIP) data from ENCODE [25] to identify RBPs, including HNRNPA1,
112 HNRNPC, HNRNPL, HNRNPM, HNRNPU, and HNRNPUL1, that interact with known
113 ASAR RNAs. We also found that an ~7 kb region within the ~185 kb ASAR6-141 RNA
114 has a surprisingly high density of interacting RBPs, and that genetic deletion of this ~7kb
115 "RBP domain" from the endogenous *ASAR6-141* gene results in a delayed replication
116 timing phenotype that is comparable to deletion of the entire ~185 kb *ASAR6-141* gene
117 located on human chromosome 6. In addition, ectopic integration of transgenes,
118 expressing the ~7 kb RBP domain, into autosomes or into the inactive X chromosome
119 results in retention of the RNA within the chromosome territory of the integrated
120 chromosomes, and results in DRT/DMC, and chromosome structure instability in *cis*.
121 Taken together, these results indicate that the ~7 kb RBP domain represents a critical
122 region within the *ASAR6-141* gene that controls replication timing of human chromosome
123 6.

124 Because ASARs were identified as critical *cis*-acting elements that control
125 chromosome-wide replication timing, we tested if ASAR associated RBPs also control
126 replication timing. We found that shRNA mediated depletion of 9 different ASAR-
127 associated RBPs (HNRNPA1, HNRNPC, HNRNPL, HNRNPM, HNRNPU, HNRNPUL1,
128 HLTF, KHSRP or UCHL5) dramatically altered the normally synchronous replication
129 timing program of all autosome pairs, recapitulating the effect of individual ASAR gene
130 knockouts on a genome-wide scale.

131 Many recent studies have revealed a surprisingly dynamic and stochastic nature of
132 chromatin in eukaryotic nuclei, which is reminiscent of a multiphase fluid behavior [26-28],
133 exampled by the 40S hnRNP particle that forms a nuclear biomolecular condensate,

134 consistent with the participation in liquid–liquid phase separation [LLPS; [23]]. In addition,
135 disruption of the nuclear LLPS using brief exposure to 1,6-hexanediol results in alterations
136 of higher order chromatin organization in living cells [29,30]. Here, we found that a brief
137 exposure of cells to 1,6-hexanediol interfered with the chromosome territory localization
138 of multiple ASAR RNAs as well as C0T-1 RNA. We also found that new RNA synthesis
139 is required for recovery of the chromosome territory association of C0T-1 RNA following
140 1,6-hexanediol exposure. In summary, these results indicate that ASAR RNAs serve as
141 essential RNA scaffolds for the assembly of hnRNP/RBP complexes that function in
142 normal chromosome replication timing, and in the maintenance of structural integrity of
143 each mammalian autosome.
144

145 **Results**

146 All of the eight genetically validated ASAR genes are subject to AEI and express
147 lncRNAs that remain associated with the chromosome territories where they are
148 transcribed [4-7]. Examples of mono-allelic expression and chromosome territory
149 localization of ASAR6-141 RNA are shown in Figure 1A and 1B, where ASAR6-141 RNA
150 is within one of the chromosome 6 territories in two different cell types, male HTD114
151 cells and female GM12878 cells, respectively. We note that the size of the RNA
152 hybridization signals detected by all ASAR probes are variable, ranging in size from large
153 clouds that occupy entire chromosome territories, with similarity in appearance to XIST
154 RNA “clouds” (Fig. 1B), to relatively small sites of hybridization that remain tightly
155 associated with the expressed alleles [4-7].

156 We first sought to identify RBPs that interact with the known ASAR RNAs. Using
157 publicly available eCLIP data for 150 RBPs in K562 and HepG2 cells (ENCODE; [25,31]),
158 we identified RBP interactions within 4 ASAR genes (*ASAR1-187, ASAR6-141, ASAR8-*
159 *2.7,* and *ASAR9-23*). Utilizing the eCLIP peaks previously identified by ENCODE [25] we
160 found significant RBP binding peaks for 99 different RBPs that map within the four ASAR
161 RNAs (Table S1). We also utilized a "region-based" method to identify significant
162 enrichments of eCLiP reads against matched controls in 10 kb windows across the four
163 ASAR genes ([31]; Table S2). An example of this analysis is shown in Figure 1C, where
164 *ASAR6-141* displays significant RBP interactions for 35 different RBPs across the
165 transcribed region. Given the contiguous expression (RNAseq from total RNA) across the
166 ~185 kb *ASAR6-141* gene in both K562 and HepG2 cell lines (Fig. 1G) and the abundant
167 eCLIP reads from 35 different RBPs in 10 kb windows across the *ASAR6-141* gene (Fig.
168 1C and 1D; see Table S2), we were surprised to detect an ~7 kb region that contained
169 virtually all of the significant eCLIP peaks in both cell lines (Fig.1G; and Table S1). The
170 zoomed in view in Figure 1G shows alignment of 58 independent eCLIP peaks of RBP
171 interactions within the ~7kb RNA Binding Protein Domain (RBPD). Figure 1E shows the
172 23 RBPs with the most abundant peaks of eCLIP reads within the ~7kb RBPD.
173

174 **Disruption of the ~7kb RBPD within ASAR6-141 results in delayed replication.**

175 To determine if the ~7kb RBPD within the *ASAR6-141* gene contains replication timing
176 activity, we used CRISPR/Cas9 mediated engineering to delete the ~7 kb sequence from
177 the endogenous locus on human chromosome 6. For this analysis we designed single
178 guide RNAs (sgRNAs) to unique sequences on either side of the ~7kb RBPD (see Fig.

179 1G; and Fig. S1). We expressed these sgRNAs in combination with Cas9 in human
180 HTD114 cells and screened clones for deletion of the ~7kb RBPD (see Fig. S1). We
181 chose HTD114 cells for this analysis because they maintain mono-allelic expression and
182 asynchronous replication of both imprinted and random monoallelic genes, they have a
183 stable karyotype that does not change significantly following transfection, drug selection
184 and sub-cloning, and knockouts of the eight known ASAR genes, including *ASAR6-141*,
185 result in DRT/DMC and chromosome structure instability in *cis* [4-9,32,33]. Because *ASAR6-*
186 *141* expression is mono-allelic in the HTD114 cells [see Fig. 1A; and [5]], we isolated clones
187 that had heterozygous or homozygous deletions of the ~7kb RBPD. We determined which
188 alleles were deleted based on retention of different base pairs of a heterozygous SNP
189 located within the ~7kb RBPD (see Fig. S1 and Table S3).

190 To assay replication timing of homologous chromosome pairs we quantified DNA
191 synthesis in mitotic cells using a BrdU terminal label assay (Fig. 2A; and [34,35]). In addition,
192 the HTD114 cells contain a centromeric polymorphism on chromosome 6, which allows
193 for an unambiguous distinction between the two chromosome 6 homologs ([7-9]; also see
194 Fig. 2B). For simplicity, we refer to the chromosome 6 with the larger centromere as
195 CHR6A and to the chromosome 6 with the smaller centromere as CHR6B. From our
196 previous studies we knew that the chromosome 6 with the smaller centromere is linked
197 to the expressed allele of *ASAR6-141* [5]. Figure 2B and 2C shows the replication timing
198 analysis on a mitotic cell where the ~7kb RBPD was deleted from the expressed allele
199 (CHR6B). Note that CHR6B contains more BrdU incorporation than CHR6A, indicating
200 later replication of CHR6B (Fig. 2D). Quantification of the BrdU incorporation in CHR6B
201 and CHR6A in multiple cells indicated that deletion of the ~7kb RBPD from the expressed

202 allele resulted in a significant delay in replication timing (Fig. 2E). This is in contrast to
203 cells prior to deletion, or in cells containing a deletion of the ~7kb RBPD from the silent
204 allele (CHR6A), where the BrdU incorporation is comparable between CHR6A and
205 CHR6B (Fig. 2E). In addition, an asynchronous replication pattern was also present in
206 cells with homozygous deletions of the 7kb RBPD, with CHR6B representing the later
207 replicating allele (Fig. 2E). Furthermore, we found that the delayed replication associated
208 with deletion of the ~7kb RBPD on CHR6B is comparable to the delayed replication
209 associated with deletion of the entire *ASAR6-141* gene from the same chromosome
210 (CHR6B; Fig. 2E; also see [5]). These results indicate that the ~7kb RBPD contains
211 functional sequences for controlling replication timing, and further supports the conclusion
212 that the expressed allele but not the silent allele controls replication timing of human
213 chromosome 6 [5].
214
215 **Ectopic integration of transgenes expressing the ~7kb RBPD into autosomes.**
216 To determine if the ~7 kb RBPD is sufficient to induce delayed replication in an
217 ectopic integration assay, we generated two transgenes containing the ~7kb RBPD, one
218 in the sense orientation and one in the antisense orientation with respect to the promoter
219 (Fig. 2F). These transgenes were introduced into mouse cells and individual clones
220 isolated. We initially screened individual clones for expression of the transgenes using
221 RNA FISH with the ~7kb RBPD as probe. Because the mouse cells that we used are
222 female, we included an RNA FISH probe for Xist to serve as positive control for the RNA
223 FISH assays. This two-color RNA FISH assay allowed us to identify clones with single
224 sites of transgene expression, and allowed us to directly compare the RNA FISH signals

225 from the transgenes to that of the endogenous Xist RNA expressed from the inactive X
226 chromosome. Figure 2 shows examples of the RNA FISH signals in cells expressing
227 either the sense (Fig. 2G) or antisense (Fig. 2H) transgenes. Large clouds of RNA FISH
228 hybridization signals that are comparable to Xist RNA hybridization signals were detected
229 in 4 out of 12 clones expressing the sense transgene (Fig. 2G). In contrast, 0 out of 12
230 clones containing the antisense transgene expressed RNA FISH hybridization signals
231 comparable to Xist RNA signals, but instead only small pinpoint sites of RNA FISH
232 hybridization were detected (Fig. 2H). Note that the mouse cells are tetraploid and contain
233 two Xist RNA hybridization signals.

234 To identify the mouse chromosomes that contain the transgenes, we used DNA FISH
235 using the ~7kb RBPD DNA as probe in combination with the inverted DAPI banding
236 pattern to identify the mouse chromosomes in metaphase spreads. We then confirmed
237 the identity of the mouse chromosomes using DNA FISH on metaphase spreads using
238 the ~7kb RBPD in combination with BAC probes from the chromosomes of interest. For
239 example, clone ~7kb(+)A5, which contains the sense-strand transgene integrated in
240 mouse chromosome 5 is shown in Figure S2A. Next, to determine if the RNA expressed
241 from the ~7kb RBPD sense strand transgene is retained within the chromosome territory
242 that expresses the transgene, we used RNA-DNA FISH with the ~7kb RBPD as RNA
243 probe plus a chromosome paint to detect mouse chromosome 5 DNA in clone ~7kb(+)A5.
244 Figure 2I shows that the ~7kb RBPD RNA is localized within one of the chromosome 5
245 DNA hybridization signals, indicating that the ~7kb RBPD RNA is retained within the
246 chromosome 5 territory.

247 Next to determine if the ~7kb RBPD transgene alters replication timing of mouse
248 chromosome 5, we visualized DNA synthesis in mitotic cells using the BrdU terminal label
249 assay [see Fig. 2A; and [34,35]]. Cells were exposed to BrdU for five hours, harvested for
250 mitotic cells, and processed for BrdU incorporation and for DNA FISH using the ~7kb
251 RBPD transgene to identify the integrated chromosome. Figure 2J shows an example of
252 this replication-timing assay in a mitotic cell containing the ~7kb RBPD sense strand
253 transgene integrated into mouse chromosome 5. Note that the chromosome containing
254 the ~7kb RBPD transgene is delayed in mitotic condensation and contains more BrdU
255 incorporation than any other chromosome within the same cell. In contrast, integration of
256 the transgene with the ~7kb RBPD in the antisense orientation did not result in delayed
257 condensation nor in delayed replication of mouse chromosomes (Fig. 2K).
258
259 **Depletion of RBPs disrupts the chromosome territory localization of ASAR RNAs.**
260 The results described above identified 99 RBPs expressed in two different cell lines
261 that interact with four different ASAR RNAs (see Table S1). Next, to determine if the
262 ASAR associated RBPs function in the chromosome territory localization of ASAR RNAs,
263 we analyzed ASAR RNA localization in cells with shRNA depletion of 12 different RBPs.
264 Figure 3A-J shows examples of antibody staining for HNRNPU, HNRNPUL1, HNRNPC,
265 HNRNPM, and HLTF in K562 cells expressing either empty vector or vectors expressing
266 shRNAs to individual RBPs. Quantitation of the immunofluorescence for each RBP in
267 empty vector versus shRNA expressing cells, indicated a significant depletion of each
268 RBP (Fig. 3K; also see Fig. S3 for Western blots).

269 Next, to determine if the nuclear localization of ASAR6-141 RNA was affected by RBP
270 depletions we used RNA FISH assays in K562 cells expressing shRNAs against the 12
271 RBPs. For this analysis we used RNA FISH to detected ASAR6-141 RNA, and because
272 K562 cells are female we also included a probe for XIST RNA as control for the RNA
273 FISH. Figure 3L shows the expected RNA FISH patterns for both ASAR6-141 and XIST
274 RNAs in cells expressing empty vector. In contrast, cells expressing shRNAs directed at
275 HNRNPU, HNRNPUL1, HNRNPC, HNRNPM, HLTF, HNRNPA1, HNRNPL, KHSRP, or
276 UCHL5 showed a nearly complete absence of the highly localized nuclear RNA
277 hybridization signals for ASAR6-141 RNA, and the appearance of large punctate
278 cytoplasmic hybridization signals (Fig. 3M-U). We also noticed an overall increase in a
279 diffuse ASAR6-141 RNA nuclear and cytoplasmic hybridization signal. In contrast, cells
280 expressing shRNAs directed at PTBP1, PTBP2, or MATR3 showed only the typical
281 nuclear localized hybridization signals for both ASAR6-141 and XIST RNAs (Fig. 3V; and
282 Fig. S4A-D). In addition, localized nuclear XIST RNA hybridization signals were detected
283 in all shRNA treated cells (Fig. 3M-V and Fig. S4A-D). However, we detected cytoplasmic
284 foci of XIST RNA hybridization that colocalized with the ASAR6-141 RNA, and a
285 significant decrease in the size of the nuclear XIST RNA hybridization signals (Fig. 3W).
286 These observations indicate that at least some of the XIST RNA was dissociated from the
287 inactive X chromosome and colocalized with ASAR6-141 RNA in large cytoplasmic foci.
288

289 **Ectopic integration of the ~7kb RBPD transgene into the inactive X chromosome.**

290 The results described above indicate that shRNA depletion of 9 different RBPs resulted
291 in dissociation of ASAR6-141 RNA from its parent chromosome, and resulted in a

292 decreased nuclear XIST RNA hybridization signal with concomitant colocalization of both
293 RNAs in cytoplasmic foci (see Fig. 3), suggesting that ASAR6-141 and XIST RNAs are
294 retained on their respective chromosome territories via similar mechanisms, which is
295 supported by the large overlap in RBPs associated with both RNAs (Fig. 1E and 1F; and
296 Table S1). In addition, ectopic integration of *Xist* transgenes into autosomes has been an
297 instrumental tool in characterization of *Xist* functions, including the ability to delay
298 replication timing and induce gene silencing [36-38]. Therefore, we next sought to determine
299 the consequences of ectopic integration of the ASAR6-141 ~7kb RBPD transgene into
300 the inactive X chromosome. The ectopic integration assays described above involved
301 random integration of transgenes followed by an RNA FISH screen for clones expressing
302 the ~7kb RBPD, which included an RNA FISH probe for Xist RNA as positive control.
303 Therefore, to identify transgene integrations into the inactive X chromosome, we simply
304 screened an additional 50 clones for colocalization of RNA FISH hybridization signals for
305 both Xist and the ~7kb RBPD transgene. Figure 4A shows this RNA FISH assay on cells
306 where the Xist and ~7kb RBPD hybridization signals are colocalized. We note that the
307 intensity of the Xist RNA FISH signal was enhanced in the region where the ~7kb RBPD
308 hybridization signal was detected (Fig. 4B), suggesting that the presence of the ~7kb
309 RBPD RNA promoted preferential localization of Xist RNA in the same region of the X
310 chromosome territory that contains the ~7kb RBPD RNA.

311 To confirm that the mouse X chromosome contains the transgene, we used DNA FISH
312 using the ~7kb RBPD DNA as probe in combination with an X chromosome paint probe
313 on metaphase spreads. An example of this analysis is shown in Figure S2B and S2C,
314 and indicates that the ~7kb RBPD transgene is integrated into an X chromosome. During

315 this analysis we detected DMC on X chromosomes, and the X chromosomes with DMC
316 contain the ~7kb RBPD transgene (Figs. 4C and 4D).
317 Next, to determine if the ~7kb RBPD transgene alters replication timing of the inactive
318 X chromosome, we visualized DNA synthesis in mitotic cells using our BrdU terminal label
319 assay (see Fig. 2A; and [34,35]). Cells were exposed to BrdU for five hours, harvested for
320 mitotic cells, and processed for BrdU incorporation and for FISH using the ~7kb RBPD
321 transgene plus an X chromosome paint probe to identify the integrated chromosome.
322 Figure 4E-4H shows an example of delayed replication and delayed mitotic condensation
323 of the X chromosome in a mitotic cell containing the ~7kb RBPD sense transgene
324 integrated into the inactive X chromosome. We conclude that integration of the 7kb RBPD
325 transgene is sufficient to cause DRT/DMC on the inactive X chromosome.
326
327 **Disruption of the chromosome associated localization of ASAR6 and ASAR1-187**
328 **RNAs.**
329 To determine if the chromosomal localization of other ASAR RNAs was also affected
330 by RBP knockdowns we carried out RNA-DNA FISH for ASAR1-187 and ASAR6 RNAs
331 simultaneously. For this analysis we used Fosmid probes to detect the ASAR RNAs plus
332 BAC probes to detect the DNA near the ASAR genes located on chromosomes 1 and 6
333 (see Table S3). Figure 5A-5C shows this RNA FISH assay on K562 cells expressing
334 empty vector, and indicates that the RNA FISH signals for both ASARs are closely
335 associated with the DNA FISH signals on their respective chromosomes, i.e. ASAR1-187
336 RNA shows close association with the chromosome 1 BAC DNA, and ASAR6 RNA shows
337 close association with the chromosome 6 BAC DNA. In contrast, cells with shRNA

338 depletion of HNRNPA1, HNRNPC, HNRNPL, HNRNPM, HNRNPU, HLTF, KHSRP, or
339 UCHL5 showed a dispersed punctate nuclear pattern for both ASAR RNAs (Fig. 5D-5K).
340 In addition, large punctate cytoplasmic foci were detected, with the two ASAR RNA
341 hybridization signals colocalized.

342 Next, to determine if depletion of RBPs would result in loss of the ASAR RNA
343 chromosome localization in a second cell type, we carried out RNA-DNA FISH assays on
344 shRNA depleted HTD114 cells. We chose HTD114 cells because we previously used
345 these cells to detect the chromosome territory localization of all eight ASAR RNAs and to
346 measure the synchronous replication timing of five autosome pairs both before and after
347 ASAR gene disruptions ([4-8,33]; and see Figure 2). Figure 5L-5N shows the RNA-DNA FISH
348 assay in HTD114 cells expressing empty vector. We again note the tight association of
349 the ASAR RNAs with the genomic loci where they are transcribed. In contrast, cells
350 expressing shRNA against HNRNPU show loss of the chromosome associated RNA
351 hybridization signals for both ASAR RNAs, and instead show diffuse nuclear and
352 cytoplasmic hybridization, with the presence of large punctate cytoplasmic foci that
353 hybridize to both ASAR RNA FISH probes (Fig. 5O-5Q). Similar results were obtained
354 following shRNA depletion of HNRNPA1, HNRNPC, HNRNPL, HNRNPM, HNRNPUL1,
355 KHSRP, HLTF, or UCHL5 (Fig. S5). In contrast, expression of shRNAs against SAFB,
356 SAFB2, SAFB plus SAFB2, CTCF, or MATR3 did not alter the ASAR1-187 or ASAR6
357 RNA nuclear hybridization signals in HTD114 cells (Fig. S4E-S4J).

358

359 **Depletion of RBPs causes asynchronous replication on all autosome pairs.**

360 Next, to determine if ASAR associated RBPs function during the normally synchronous
361 replication timing program that occurs on pairs of homologous chromosomes, we
362 analyzed DNA synthesis in HTD114 cells depleted for the 9 RBPs implicated in ASAR
363 RNA localization (HNRNPU, HNRNPA1, HNRNPC, HNRNPL, HNRNPM, HNRNPUL1,
364 KHSRP, HLTF, or UCHL5) and for the five RBPs that showed no effect on ASAR RNA
365 localization (MATR3, PTBP1, PTBP2, SAFB, or SAFB2). Using the BrdU terminal label
366 assay [34,35] in cells expressing the empty vector, we found that each autosome pair
367 displays a typical synchronous BrdU incorporation pattern for each autosome pair (Fig.
368 6A). In contrast, following HNRNPU depletion, individual mitotic spreads displayed
369 dramatic differential incorporation of BrdU into pairs of homologous chromosomes,
370 examples of asynchronous replication timing between every pair of autosomes are shown
371 in Figure 6B. Note that each chromosome pair contains dramatic differential BrdU
372 incorporation into chromosome homologs, which represents considerable asynchronous
373 replication timing. Figure 6C and 6D show examples for chromosome pairs 4 and 18 (also
374 see Fig. S6C). Quantification of the BrdU incorporation in chromosomes 1 and 6 (see Fig.
375 S6) in multiple cells depleted for HNRNPU, HNRNPUL1, HLTF, KHSRP, UCHL5, or
376 HNRNPA1 indicated that both pairs of chromosomes display significant asynchrony (Fig.
377 6E and 6F). In addition, the DRT/DMC phenotype was detected in ~30% of mitotic
378 spreads following shRNA-mediated depletions (two examples are shown in Fig. 6G and
379 6H; also see Fig. S7). Furthermore, shRNA-mediated depletion of HNRNPC, HNRNPL
380 and HNRNPM resulted in dramatic alterations in chromosome morphology that included
381 asynchronous replication and abnormal mitotic condensation, including ~10% of mitotic

382 spreads with one or more chromosomes that displayed the DRT/DMC phenotype (Fig.
383 S7).
384
385 **A brief exposure to 1,6-hexanediol disrupts ASAR and C0T-1 RNA localization.**
386 Recent studies have found that the 40S hnRNP particle, which contains HNRNPA1
387 and HNRNPC, forms a nuclear biomolecular condensate, consistent with participation in
388 LLPS [23]. The shRNA depletion assays described above resulted in mislocalization of
389 multiple ASAR RNAs into punctate foci, which is suggestive of LLPS. To determine if 1,6-
390 hexanediol can disrupt the chromosome territory localization of ASAR RNAs we exposed
391 HTD114 cells to 4% 1,6-hexanediol for 20 minutes, and then processed the cells for RNA-
392 DNA FISH. Figure 7 shows this analysis and indicates that the chromosome territory
393 localization of ASAR1-187, ASAR6, and ASAR6-141 RNAs is disrupted in cells exposed
394 to 1,6-hexanediol, with all three RNAs being detected as diffuse hybridization patterns in
395 the nucleus and cytoplasm. We note a dramatic increase in the nuclear and cytoplasmic
396 RNA hybridization signals for all three ASAR RNAs. In addition, washing out the 1,6-
397 hexanediol and allowing the cells to recover for 4 hours revealed that the ASAR RNAs
398 regained their normal localization patterns at their respective chromosomal loci (Fig. 7C,
399 7F, and 7I).
400 Next, to determine the relationship between the RNA species detected by C0T-1 DNA
401 and ASAR RNAs in RNA FISH assays, we used human C0T-1 DNA as an RNA FISH
402 probe on mouse cells expressing an *ASAR6* BAC transgene [8]. Because human C0T-1
403 DNA does not cross hybridize with mouse RNA or DNA in FISH assays [20], we were able
404 to detect the chromosome territory localized expression of human ASAR6 RNA

405 expressed from the transgene that is integrated into mouse chromosome 3 using human
406 C0T-1 DNA as RNA FISH probe (Fig. 8A and 8B), indicating that C0T-1 DNA detects
407 ASAR6 RNA.

408 Next to determine if a brief exposure of cells to 1,6-hexanediol can disrupt the
409 chromosome territory localization of C0T-1 RNA, we exposed GM11687 cells, which are
410 mouse A9 hybrid cells containing human chromosome 4, to 4% 1,6-hexanediol for 20
411 minutes and then processed the cells for RNA-DNA FISH. Figure 8 shows this analysis
412 and indicates that the chromosome territory localization of human C0T-1 RNA is disrupted
413 in cells exposed to 1,6-hexanediol, and that the human C0T-1 RNA is detected as a
414 diffuse hybridization pattern in the nucleus and cytoplasm (Fig. 8C and 8D). In addition,
415 washing out the 1,6-hexanediol and allowing the cells to recover for 4 hours revealed that
416 the human C0T-1 RNA regained its normal chromosome territory localization pattern (Fig.
417 8E).

418 Next, to determine if new RNA synthesis is required to reestablish the chromosome
419 territory localization of human C0T-1 RNA, we treated cells with 1,6-hexanediol for 20
420 minutes, washed out the 1,6-hexanediol and allowed the cells to recover for 4 hours either
421 in the presence or absence of Actinomycin D. Figure 8F and 8G shows this analysis and
422 indicates that human C0T-1 RNA was not detected on the human chromosome territory
423 in cells treated with 1,6-hexanediol and allowed to recover for 4 hours in the presence of
424 Actinomycin D. We note that a 4-hour exposure of cells to Actinomycin D without a prior
425 exposure to 1,6-hexanediol had no effect on the association of C0T-1 RNA to the human
426 chromosome territory (Fig. 8H). Taken together, these observations indicate 1,6-
427 hexanediol exposure disrupts the ASAR and C0T-1 RNA localization to chromosome

428 territories, and that new RNA synthesis is required for the generation of the chromosome
429 territory localization of C0T-1 RNA.
430
431 **Discussion:**
432 We recently identified 68 ASAR candidate genes, and genetically validated five out of five
433 as controlling replication timing of individual human autosomes, bringing the total of
434 genetically validated ASAR genes to eight [4-7]. These eight ASAR genes (*ASAR1-187,*
435 *ASAR6, ASAR6-141, ASAR8-2.7, ASAR9-23, ASAR9-24, ASAR9-30 and ASAR15*)
436 display striking epigenetically controlled allelic expression and replication timing, and their
437 RNAs remain localized to their parent chromosome territories [4-7]. In this report, we used
438 publicly available RNA-protein interaction data from ENCODE to identify RBPs that
439 interact with multiple ASAR RNAs. One unanticipated observation that came from this
440 analysis was that an ~7 kb domain within the ~185 kb ASAR6-141 RNA contained virtually
441 all of the significant peaks of RBP interactions in two different cell lines. Using genetic
442 deletion and ectopic integration assays we found that this ~7kb RBPD contains functional
443 sequences for controlling replication timing of entire chromosomes in *cis*. We also found
444 that shRNA-mediated depletion of 9 different ASAR-associated RBPs results in loss of
445 the chromosome territory association of multiple ASAR RNAs. In addition, we found that
446 depletion of HNRNPA1, HNRNPC, HNRNPL, HNRNPM, HNRNPU, HNRNPUL1, HLTF,
447 KHSRP, or UCHL5 alters the normally synchronous replication timing that occurs
448 between pairs of homologous chromosomes resulting in the DRT/DMC phenotype,
449 recapitulating the effect of individual ASAR gene knockouts on a genome-wide scale.
450 Furthermore, we found that a brief exposure of cells to 1,6-hexanediol disrupts the

451 chromosome territory localization of multiple ASAR and C0T-1 RNAs, and that new RNA
452 synthesis is required to restore the chromosome territory localization of C0T-1 RNA.
453 Previous studies have suggested that C0T-1 RNA plays a dynamic structural role that
454 promotes the open architecture of active chromosome territories [13,20]. C0T-1 RNA is
455 predominantly L1 sequences, and these L1 RNAs remain associated with the
456 chromosome territories where they are transcribed [20]. Additional studies have proposed
457 that repRNA is an important regulator of the dynamic organization of genomic loci into
458 membrane-less subcompartments with distinct nuclear functions (reviewed in [19]). Other
459 studies have proposed that HNRNPU nonspecifically interacts with "RNA debris" to create
460 a dynamic nuclear mesh that regulates interphase chromatin structure [12,18]. One
461 important distinction that can be made between ASAR RNAs and these other hnRNAs
462 (i.e. C0T-1 RNA, repRNA, caRNA, and "RNA debris" [12,13,18-21]) is that ASARs have been
463 defined genetically, and these other RNAs have not. Thus, we have used both loss of
464 function and gain of function assays to define the roles that ASAR genes play in
465 chromosome dynamics, which includes control of chromosome-wide replication timing
466 and mitotic chromosome condensation [4-8]. We also found that C0T-1 DNA, when used as
467 an RNA FISH probe, can detect ASAR6 RNA that is expressed and localized to an
468 individual chromosome territory, suggesting that at least some of the RNA FISH signal
469 detected by C0T-1 DNA represents ASARs. In addition, we found that a brief exposure
470 to 1,6-hexanediol disrupts the chromosome territory localization of multiple ASAR RNAs,
471 suggesting that ASAR RNAs participate in the nuclear LLPS processes that helps to
472 organize chromosome territories. Given our recent discovery of ASAR RNAs expressed
473 from every autosome, and encoded by ~3% of the human genome [6], we propose that

474 ASAR RNAs represent functional “chromosome associated RNA” species that control
475 chromosome dynamics within mammalian nuclei. Whether or not there are nuclear
476 functions of other chromosome associated hnRNAs that are independent of ASARs will
477 require genetic and/or functional validation.

478 Here we identified several hnRNPs (HNRNPA1, HNRNPC, HNRNPL, HNRNPM,
479 HNRNPU, and HNRNPUL1) as important interaction partners for the chromosome
480 territory localization of multiple ASAR RNAs. In addition, we found that the SWI/SNF
481 related transcription factor HLTF, which was recently shown to regulate replication fork
482 reversal, prevent alternative mechanisms of stress-resistant DNA replication, and
483 mediates cellular resistance to replication stress [39], is required for the chromosome
484 territory localization of multiple ASAR RNAs and for the synchronous replication of every
485 autosome pair. Furthermore, we found that the KH domain (HNRNPK Homology domain)
486 containing protein KHSRP, and the ubiquitin hydrolase UCHL5 also contribute to the
487 chromosome territory localization of ASAR RNAs. We found that depletion of HNRNPA1,
488 HNRNPC, HNRNPL, HNRNPM, HNRNPU, HNRNPUL1, HLTF, KHSRP, or UCHL5
489 proteins resulted in a dramatic genome-wide disruption of the normally synchronous
490 replication timing program on all autosome pairs. Taken together our results indicate that
491 the association of ASAR RNAs with multiple hnRNPs in combination with other nuclear
492 RBPs is an essential step in the regulation of the synchronous replication timing program
493 on mammalian chromosomes.

References:

1. Mukhopadhyay, R., Lajugie, J., Fourel, N., Selzer, A., Schizas, M., Bartholdy, B., Mar, J., Lin, C.M., Martin, M.M., Ryan, M., et al. (2014). Allele-specific genome-wide profiling in human primary erythroblasts reveal replication program organization. PLoS Genet *10*, e1004319. 10.1371/journal.pgen.1004319.
2. Dileep, V., and Gilbert, D.M. (2018). Single-cell replication profiling to measure stochastic variation in mammalian replication timing. Nature communications *9*, 427. 10.1038/s41467-017-02800-w.
3. Rivera-Mulia, J.C., Dimond, A., Vera, D., Trevilla-Garcia, C., Sasaki, T., Zimmerman, J., Dupont, C., Gribnau, J., Fraser, P., and Gilbert, D.M. (2018). Allele-specific control of replication timing and genome organization during development. Genome Res *28*, 800-811. 10.1101/gr.232561.117.
4. Donley, N., Smith, L., and Thayer, M.J. (2015). ASAR15, A cis-Acting Locus that Controls Chromosome-Wide Replication Timing and Stability of Human Chromosome 15. PLoS Genet *11*, e1004923. 10.1371/journal.pgen.1004923.
5. Heskett, M.B., Smith, L.G., Spellman, P., and Thayer, M.J. (2020). Reciprocal monoallelic expression of ASAR lncRNA genes controls replication timing of human chromosome 6. RNA (New York, N.Y.) *26*, 724-738. 10.1261/rna.073114.119.
6. Heskett, M.B., Vouzas, A.E., Smith, L.G., Yates, P.A., Boniface, C., Bouhassira, E.E., Spellman, P.T., Gilbert, D.M., and Thayer, M.J. (2022). Epigenetic control of chromosome-associated lncRNA genes essential for replication and stability. Nature communications *13*, 6301. 10.1038/s41467-022-34099-7.
7. Stoffregen, E.P., Donley, N., Stauffer, D., Smith, L., and Thayer, M.J. (2011). An autosomal locus that controls chromosome-wide replication timing and mono-allelic expression. Hum Mol Genet *20*, 2366-2378.
8. Donley, N., Stoffregen, E.P., Smith, L., Montagna, C., and Thayer, M.J. (2013). Asynchronous Replication, Mono-Allelic Expression, and Long Range Cis-Effects of ASAR6. PLoS Genet *9*, e1003423.
9. Platt, E.J., Smith, L., and Thayer, M.J. (2018). L1 retrotransposon antisense RNA within ASAR lncRNAs controls chromosome-wide replication timing. J Cell Biol *217*, 541-553. 10.1083/jcb.201707082.
10. Ding, D.Q., Okamasa, K., Katou, Y., Oya, E., Nakayama, J.I., Chikashige, Y., Shirahige, K., Haraguchi, T., and Hiraoka, Y. (2019). Chromosome-associated RNA-protein complexes promote pairing of homologous chromosomes during meiosis in Schizosaccharomyces pombe. Nature communications *10*, 5598. 10.1038/s41467-019-13609-0.
11. Faber, M.W., and Vo, T.V. (2022). Long RNA-Mediated Chromatin Regulation in Fission Yeast and Mammals. Int J Mol Sci *23*. 10.3390/ijms23020968.
12. Nozawa, R.S., and Gilbert, N. (2019). RNA: Nuclear Glue for Folding the Genome. Trends Cell Biol *29*, 201-211. 10.1016/j.tcb.2018.12.003.
13. Creamer, K.M., Kolpa, H.J., and Lawrence, J.B. (2021). Nascent RNA scaffolds contribute to chromosome territory architecture and counter chromatin compaction. Mol Cell. 10.1016/j.molcel.2021.07.004.

538 14. Menon, D.U., and Meller, V.H. (2015). Identification of the Drosophila X
539 chromosome: The long and short of it. RNA biology *12*, 1088-1093.
540 10.1080/15476286.2015.1086864.
541 15. St Laurent, G., Savva, Y.A., and Kapranov, P. (2012). Dark matter RNA: an
542 intelligent scaffold for the dynamic regulation of the nuclear information
543 landscape. Frontiers in genetics *3*, 57. 10.3389/fgene.2012.00057.
544 16. Kristensen, L.S., Andersen, M.S., Stagsted, L.V.W., Ebbesen, K.K., Hansen,
545 T.B., and Kjems, J. (2019). The biogenesis, biology and characterization of
546 circular RNAs. Nat Rev Genet *20*, 675-691. 10.1038/s41576-019-0158-7.
547 17. St Laurent, G., Vyatkin, Y., Antonets, D., Ri, M., Qi, Y., Saik, O., Shtokalo, D., de
548 Hoon, M.J., Kawaji, H., Itoh, M., et al. (2016). Functional annotation of the vlinc
549 class of non-coding RNAs using systems biology approach. Nucleic Acids
550 Research. 2 *44*, 3233-3252. 10.1093/nar/gkw162.
551 18. Nozawa, R.S., Boteva, L., Soares, D.C., Naughton, C., Dun, A.R., Buckle, A.,
552 Ramsahoye, B., Bruton, P.C., Saleeb, R.S., Arnedo, M., et al. (2017). SAF-A
553 Regulates Interphase Chromosome Structure through Oligomerization with
554 Chromatin-Associated RNAs. Cell *169*, 1214-1227.e1218.
555 10.1016/j.cell.2017.05.029.
556 19. Frank, L., and Rippe, K. (2020). Repetitive RNAs as Regulators of Chromatin-
557 Associated Subcompartment Formation by Phase Separation. J Mol Biol *432*,
558 4270-4286. 10.1016/j.jmb.2020.04.015.
559 20. Hall, L.L., Carone, D.M., Gomez, A.V., Kolpa, H.J., Byron, M., Mehta, N.,
560 Fackelmayer, F.O., and Lawrence, J.B. (2014). Stable C0T-1 repeat RNA is
561 abundant and is associated with euchromatic interphase chromosomes. Cell *156*,
562 907-919. 10.1016/j.cell.2014.01.042.
563 21. Kolpa, H.J., Creamer, K.M., Hall, L.L., and Lawrence, J.B. (2021). SAF-A
564 mutants disrupt chromatin structure through dominant negative effects on RNAs
565 associated with chromatin. Mamm Genome. 10.1007/s00335-021-09935-8.
566 22. Geuens, T., Bouhy, D., and Timmerman, V. (2016). The hnRNP family: insights
567 into their role in health and disease. Hum Genet *135*, 851-867. 10.1007/s00439-
568 016-1683-5.
569 23. Domanski, M., Dedic, E., Pérez, M.E., Cléry, A., Campagne, S., Uldry, A.C.,
570 Braga, S., Heller, M., Rabl, J., Afanasyev, P., et al. (2022). 40S hnRNP particles
571 are a novel class of nuclear biomolecular condensates. Nucleic Acids Research.
572 2 *50*, 6300-6312. 10.1093/nar/gkac457.
573 24. Connolly, C., Takahashi, S., Miura, H., Hiratani, I., Gilbert, N., Donaldson, A.D.,
574 and Hiraga, S.I. (2022). SAF-A promotes origin licensing and replication fork
575 progression to ensure robust DNA replication. J Cell Sci *135*.
576 10.1242/jcs.258991.
577 25. Moore, J.E., Purcaro, M.J., Pratt, H.E., Epstein, C.B., Shoresh, N., Adrian, J.,
578 Kawli, T., Davis, C.A., Dobin, A., Kaul, R., et al. (2020). Expanded
579 encyclopaedias of DNA elements in the human and mouse genomes. Nature
580 *583*, 699-710. 10.1038/s41586-020-2493-4.
581 26. Laghmach, R., Di Pierro, M., and Potoyan, D.A. (2021). The interplay of
582 chromatin phase separation and lamina interactions in nuclear organization.
583 Biophys J *120*, 5005-5017. 10.1016/j.bpj.2021.10.012.

27. Laghmach, R., Di Pierro, M., and Potoyan, D. (2021). A Liquid State Perspective on Dynamics of Chromatin Compartments. Front Mol Biosci *8*, 781981. 10.3389/fmolb.2021.781981.
28. Rippe, K. (2022). Liquid-Liquid Phase Separation in Chromatin. Cold Spring Harb Perspect Biol *14*. 10.1101/cshperspect.a040683.
29. Ulianov, S.V., Velichko, A.K., Magnitov, M.D., Luzhin, A.V., Golov, A.K., Ovsyannikova, N., Kireev, II, Gavrikov, A.S., Mishin, A.S., Garaev, A.K., et al. (2021). Suppression of liquid-liquid phase separation by 1,6-hexanediol partially compromises the 3D genome organization in living cells. Nucleic Acids Research. 2 *49*, 10524-10541. 10.1093/nar/gkab249.
30. Liu, X., Jiang, S., Ma, L., Qu, J., Zhao, L., Zhu, X., and Ding, J. (2021). Time-dependent effect of 1,6-hexanediol on biomolecular condensates and 3D chromatin organization. Genome Biol *22*, 230. 10.1186/s13059-021-02455-3.
31. Van Nostrand, E.L., Pratt, G.A., Shishkin, A.A., Gelboin-Burkhart, C., Fang, M.Y., Sundararaman, B., Blue, S.M., Nguyen, T.B., Surka, C., Elkins, K., et al. (2016). Robust transcriptome-wide discovery of RNA-binding protein binding sites with enhanced CLIP (eCLIP). Nat Methods *13*, 508-514. 10.1038/nmeth.3810.
32. Chang, B.H., Smith, L., Huang, J., and Thayer, M. (2007). Chromosomes with delayed replication timing lead to checkpoint activation, delayed recruitment of Aurora B and chromosome instability. Oncogene *26*, 1852-1861.
33. Breger, K.S., Smith, L., and Thayer, M.J. (2005). Engineering translocations with delayed replication: evidence for cis control of chromosome replication timing. Hum Mol Genet *14*, 2813-2827.
34. Smith, L., Plug, A., and Thayer, M. (2001). Delayed Replication Timing Leads to Delayed Mitotic Chromosome Condensation and Chromosomal Instability of Chromosome Translocations. Proc Natl Acad Sci U S A *98*, 13300-13305.
35. Smith, L., and Thayer, M. (2012). Chromosome replicating timing combined with fluorescent in situ hybridization. J Vis Exp *10*, e4400.
36. Minks, J., and Brown, C.J. (2009). Getting to the center of X-chromosome inactivation: the role of transgenes. Biochem Cell Biol *87*, 759-766.
37. Pintacuda, G., Wei, G., Roustan, C., Kirmizitas, B.A., Solcan, N., Cerase, A., Castello, A., Mohammed, S., Moindrot, B., Nesterova, T.B., and Brockdorff, N. (2017). hnRNPK Recruits PCGF3/5-PRC1 to the Xist RNA B-Repeat to Establish Polycomb-Mediated Chromosomal Silencing. Mol Cell *68*, 955-969.e910. 10.1016/j.molcel.2017.11.013.
38. Lee, J.T., Strauss, W.M., Dausman, J.A., and Jaenisch, R. (1996). A 450 kb transgene displays properties of the mammalian X-inactivation center. Cell *86*, 83-94.
39. Bai, G., Kermi, C., Stoy, H., Schiltz, C.J., Bacal, J., Zaino, A.M., Hadden, M.K., Eichman, B.F., Lopes, M., and Cimprich, K.A. (2020). HLTF Promotes Fork Reversal, Limiting Replication Stress Resistance and Preventing Multiple Mechanisms of Unrestrained DNA Synthesis. Mol Cell *78*, 1237-1251.e1237. 10.1016/j.molcel.2020.04.031.
40. Kruskal, J.B. (1964). Multidimensional scaling by optimizing goodness of fit to a nonmetric hypothesis. Psychometrika *29*, 1–27.

41. Zhu, Y., Bye, S., Stambrook, P.J., and Tischfield, J.A. (1994). Single-base deletion induced by benzo[a]pyrene diol epoxide at the adenine phosphoribosyltransferase locus in human fibrosarcoma cell lines. Mutat Res *321*, 73-79.
42. Van Nostrand, E.L., Freese, P., Pratt, G.A., Wang, X., Wei, X., Xiao, R., Blue, S.M., Chen, J.Y., Cody, N.A.L., Dominguez, D., et al. (2020). A large-scale binding and functional map of human RNA-binding proteins. Nature *583*, 711-719. 10.1038/s41586-020-2077-3.
43. Dobin, A., Davis, C.A., Schlesinger, F., Drenkow, J., Zaleski, C., Jha, S., Batut, P., Chaisson, M., and Gingeras, T.R. (2013). STAR: ultrafast universal RNA-seq aligner. Bioinformatics (Oxford, England) *29*, 15-21. 10.1093/bioinformatics/bts635.
44. Li, H., Handsaker, B., Wysoker, A., Fennell, T., Ruan, J., Homer, N., Marth, G., Abecasis, G., and Durbin, R. (2009). The Sequence Alignment/Map format and SAMtools. Bioinformatics (Oxford, England) *25*, 2078-2079. 10.1093/bioinformatics/btp352.

Figure legends

Figure 1. RNA binding proteins interact with an ~7 kb domain within ASAR6-141 RNA. A) RNA-DNA FISH images of ASAR6-141 expression in six individual HTD114 cells. ASAR6-141 RNA (green; green arrows) and chromosome 6 DNA (chromosome paint, red), and DNA was stained with DAPI. B) RNA-DNA FISH of ASAR6-141 RNA (red, red arrows), CHR6 DNA (chromosome paint, white), and XIST RNA (green, green arrows) visualized within individual GM12878 cells, top and bottom panels represent the same three cells with the nuclear outline drawn in white. C) RNA-protein interaction data (eCLIP from ENCODE) for 120 RBPs expressed in K562 cells for the genomic region that contains ASAR6-141, and ~200 kb of upstream non-transcribed DNA (chromosome 6 140.8 mb-141.6 mb). Each point represents the FDR-corrected p-value of the z-score of log2-ratio between eCLiP vs control for each RBP within a 10kb sliding window. D) Number of 10kb regions with significant enrichments of eCLiP reads vs control within ASAR6-141. E) Histogram of eCLiP peaks count per RBP within ASAR6-141 7kb RBPD. F) Histogram of eCLiP peaks count per RBP within lncRNA XIST. G) Genome browser view of *ASAR6-141* with RNA-seq expression and eCLiP peaks shown in K562 and HepG2. The zoomed in view shows the ~7kb RBPD with the location of the peaks of eCLIP reads that map within the region (see Table S1). The location of sgRNAs are shown with arrows (see Table S3), and the asterisks mark the sgRNAs from [5].

Figure 2. Replication timing in cells with *ASAR6-141 ~7kb* RBPD deletion or ectopic integration. A) Schematic illustration of the BrdU terminal label protocol [35]. Cells were treated with BrdU (green) for 5 hours and then harvested for mitotic cells. B) BrdU incorporation in HTD114 cells containing a heterozygous deletion of the ~7kb RBPD. Cells containing a deletion of the ~7kb RBPD from the expressed allele of *ASAR6-141* were exposed to BrdU, harvested for mitotic cells, and subjected to DNA FISH using a chromosome 6 centromeric probe (red; B). The larger centromere resides on the chromosome 6 with the silent *ASAR6-141* allele (CHR6A), and the smaller centromere resides on the chromosome 6 with the expressed *ASAR6-141* allele (CHR6B). DNA was stained with DAPI (blue). C and D) DAPI staining and BrdU incorporation were quantified by calculating the number of pixels (area x intensity) and displayed as a ratio of BrdU incorporation in CHR6B divided by the BrdU incorporation in CHR6A. E) Quantification of BrdU incorporation in multiple cells with heterozygous (Δ7kb-6B, expressed allele; or Δ7kb-6A, silent allele) or homozygous (Δ7kb-6B/6A) deletions of the ~7kb RBPD. Also shown is the quantification of BrdU incorporation in heterozygous deletions of the entire ~185 kb *ASAR6-141* gene from chromosome 6B (Δ185-6B) or 6A (Δ185-6A) [5]. Box plots indicate mean (solid line), standard deviation (dotted line), 25th, 75th percentile (box) and 5th and 95th percentile (whiskers) and individual cells (single points). P values were calculated using the Kruskal-Wallis test [40]. Values for individual cells are shown as dots. **P = 0.00027 and *P = 0.03. F) Schematic view of the ~7kb RBPD in both the sense and antisense orientation. The promoter used to drive expression is from the ASAR6 gene [9]. G and H) Two color RNA FISH assay for expression of the ~7kb RBPD transgenes. Individual clones were screened for RNA expressed from the ASAR6-141 (~7kb RBPD) transgenes (red, arrows), and RNA hybridization using an Xist probe (green, arrows) was used as positive control. G and H represent examples of cells containing the sense and

693 antisense transgenes, respectively. I) RNA from the ~7kb RBPD remains localized to
694 mouse chromosomes. RNA-DNA FISH using the ~7kb RBPD as RNA FISH probe (red,
695 arrows), plus a mouse chromosome 5 paint to detect chromosome 5 DNA (green,
696 brackets). J) Cells containing the sense ~7kb RBPD transgene integrated into mouse
697 chromosome 5 were exposed to BrdU (green), harvested for mitotic cells, and subjected
698 to DNA FISH using the ~7kb RBPD (red, arrows). Note that the chromosome that contains
699 the transgene shows delayed mitotic condensation and more BrdU incorporation than any
700 other chromosome within the same cell. K) Cells containing the antisense ~7kb RBPD
701 transgene integrated into mouse chromosomes were exposed to BrdU (green), harvested
702 for mitotic cells, and subjected to DNA FISH using the ~7kb RBPD (red). Note that the
703 chromosome that contains the transgene shows normal mitotic condensation and only a
704 small amount of BrdU incorporation. Scale bars are 10 uM (B, G, H) 5 uM (J, K) and 2 uM
705 (I).
706
707 **Figure 3. Depletion of RBPs results in disruption of the chromosome territory**
708 **localization of ASAR6-141 RNA.** A-J) shRNA mediated depletion of RBPs. K562 cells
709 were transfected with empty vector (A, C, E, G, and I) or vectors expressing shRNAs
710 directed against HNRNPU (B), HNRNPUL1 (D), HNRNPC (F), HNRNPM (H), or HLTF
711 (J). K) Cells were stained with the appropriate antibodies and quantitation of each RBP
712 was determined in >25 individual cells. Box plots indicate mean (solid line), standard
713 deviation (dotted line), 25th, 75th percentile (box), 5th and 95th percentile (whiskers), and
714 individual cells (single points). P values were calculated using the Kruskal-Wallis test [40].
715 L-V) RNA-DNA FISH for ASAR6-141 (green) and XIST (red) RNA. K562 cells were
716 transfected with empty vector (L) or vectors expressing shRNAs against HNRNPU (M),
717 HNRNPUL1 (N), HNRNPC (O), HNRNPM (P), HLTF (Q), HNRNPA1 (R), HNRNPL (S),
718 KHSRP (T), UCHL5 (U), or PTBP1 (V). The red arrows mark the RNA FISH signals for
719 XIST. The brackets mark cytoplasmic regions that hybridized to both RNA FISH probes.
720 DNA was stained with DAPI, and Bars are 10 *u*M (A-J and L) or 5 *u*M (M-V). W)
721 Quantitation of the XIST RNA FISH signals. K562 cells transfected and processed for
722 RNA FISH as in L-V were analyzed for quantitation of XIST RNA cloud size (pixels: area
723 X intensity) in >25 individual cells. Box plots indicate mean (solid line), standard deviation
724 (dotted line), 25th, 75th percentile (box), 5th and 95th percentile (whiskers) and individual
725 cells (single points). P values were calculated using the Kruskal-Wallis test [40].
726
727 **Figure 4. Ectopic integration of the *ASAR6-141 ~7kb RBPD* transgene into an**
728 **inactive X chromosome.** A) Two color RNA FISH assay for expression of the sense
729 ~7kb RBPD transgene plus Xist RNA. Examples of three different cells showing
730 colocalization of the ASAR RNA and Xist RNA. Individual cells were processed for
731 expression of the sense strand ~7kb RBPD transgene (left panels, red, arrow) in
732 combination with RNA FISH for Xist (middle panels, green, arrow). The right panels show
733 the merged images. The white lines show the path for the pixel intensity profiles used for
734 panel B. B) Pixel intensity profiles across the Xist RNA hybridization domain showing
735 enhanced signal intensity over the ~7kb RBPD RNA hybridization domain. C and D)
736 Delayed mitotic chromosome condensation of the X chromosome that contains the ~7kb
737 RBPD transgene. An example of a mitotic spread processed for DNA FISH using the
738 ~7kb RBPD as probe (magenta, panel C) plus a mouse X chromosome paint (red, panel

739 D). The arrows mark the location of the transgene hybridization signal. E-H) Cells
740 containing the ~7kb RBPD transgene integrated into the mouse X chromosome were
741 exposed to BrdU (G, green), harvested for mitotic cells, and subjected to DNA FISH using
742 the ~7kb RBPD (E, magenta) plus a mouse X chromosome paint (F, red). The merged
743 images are shown in panel H.
744
745 **Figure 5. Depletion of RBPs results in disruption of the chromosome territory**
746 **localization of ASAR RNAs.** shRNA mediated depletion of RBPs in K562 cells (A-K) or
747 HTD114 cells (L-Q). Cells were transfected with empty vector (A-C and L-N) or vectors
748 expressing shRNAs directed against HNRNPA1 (D), HNRNPC (E), HNRNPL (F),
749 HNRNPM (G), HNRNPU (H, and O-Q), HLTF (I), KHSRP (J), or UCHL5 (K). Cells were
750 processed for RNA FISH with probes for ASAR6 (red, arrows) and ASAR1-187 (green,
751 arrows). Cells were also processed for DNA FISH using BAC DNA to detect chromosome
752 1 (CHR1 BAC DNA, magenta) and chromosome 6 (CHR6 BAC DNA, orange; A-C and L-
753 Q). Arrows mark the sites of RNA FISH hybridization and arrowheads mark the sites of
754 DNA hybridization. RNA-DNA FISH for ASAR1-187 (RNA in green, arrows; DNA in
755 magenta and arrowheads), ASAR6 (RNA in red, arrows; DNA in orange and arrowheads).
756 The brackets mark the cytoplasmic regions that hybridized to both RNA FISH probes.
757 DNA was stained with DAPI, and scale bars are 10 *u*M.
758
759 **Figure 6. Depletion of RBPs results in asynchronous replication on autosome**
760 **pairs.** A) BrdU incorporation in parental HTD114 cells. Cells were exposed to BrdU for
761 five hours and processed for BrdU incorporation using an antibody against BrdU. This
762 panel represents chromosomes from multiple mitotic spreads showing representative
763 BrdU incorporation in chromosome pairs. Both homologs of autosome pair were captured
764 from the same mitotic cell, and each pair displays a typical BrdU incorporation pattern
765 that is consistent with synchronous replication timing. B) HTD114 cells were transfected
766 with the HNRNPU shRNA expression vector, exposed to BrdU for five hours, and
767 processed for BrdU incorporation. This panel represents chromosomes from multiple
768 mitotic spreads showing representative BrdU incorporation in pairs of autosomes. Both
769 homologs of autosome pairs were captured from the same mitotic cell, and each pair
770 displays a differential BrdU incorporation pattern that is consistent with asynchronous
771 replication timing. C) Shows two chromosome 4 homologs (CHR4A and CHR4B) side by
772 side. D) Shows the BrdU incorporation in chromosome 18 homologs (CHR18A and
773 CHR18B). For each chromosome pair the inverted DAPI staining (black and white), BrdU
774 incorporation (green), and DAPI staining (blue) are shown. E and F) Quantification of
775 BrdU incorporation in multiple cells depleted for HNRNPU, HNRNPUL1, HTLF, KHSRP,
776 UCHL5, HNRNPA1, MATR3, PTBP1, PTBP2, SAFB and SAFB2. Box plots indicate mean
777 (solid line), standard deviation (dotted line), 25th, 75th percentile (box), 5th and 95th
778 percentile (whiskers) and individual cells (single points). P values were calculated using
779 the Kruskal-Wallis test [40]. G) DRT/DMC on chromosome 6 following HNRNPU depletion.
780 HTD114 cells were transfected with the HNRNPU shRNA expression vector, exposed to
781 BrdU for 5 hours, harvested for mitotic cells, and processed for BrdU incorporation (green)
782 and DNA FISH using a chromosome 6 centromeric probe (red). H) DRT/DMC on
783 chromosome 1 following UCHL5 depletion. HTD114 cells were transfected with the
784 UCHL5 shRNA expression vector, exposed to BrdU for 5 hours, harvested for mitotic

785 cells, and processed for BrdU incorporation (green) and DNA FISH using a chromosome
786 1 paint as probe (red). The arrow marks the chromosome 1 with DRT/DMC, and the inset
787 shows only the DAPI staining of the chromosome 1 highlighting the DMC.
788
789 **Figure 7. 1,6 hexanediol disrupts the chromosome territory association of ASAR**
790 **RNAs.** HTD114 cells were exposed to 4% 1,6-hexanediol (1,6-HD) for 20 minutes,
791 washed extensively and allowed to recover for 4 hours in complete media, and processed
792 for RNA-DNA FISH. A-C) RNA FISH using an ASAR6-141 probe (green, arrows) plus a
793 BAC probe from chromosome 6 was used to detect chromosome 6 DNA (red
794 arrowheads). D-F) RNA FISH using an ASAR6 probe (green, arrows) plus a BAC probe
795 from chromosome 6 was used to detect chromosome 6 DNA (red arrowheads). G-I) RNA
796 FISH using an ASAR1-187 probe (green, arrows) plus a BAC probe from chromosome 1
797 was used to detect chromosome 1 DNA (red arrowheads). Panels A, D, and G are
798 HTD114 cells prior to exposure. B, E, and H) HTD114 cells exposed to 1,6-HD for 20
799 minutes. C, F and I) HTD114 cells exposed to 1,6-HD for 20 minutes followed by 4 hour
800 incubation in the absence of 1,6-HD (4hr recovery). DNA was stained with DAPI, and
801 scale bars are 10 *u*M.
802
803 **Figure 8. Human C0T-1 DNA detects ASAR6 RNA, and 1,6 hexanediol disrupts the**
804 **chromosome territory association of C0T-1 RNA.** A and B) RNA-DNA FISH on mouse
805 cells containing an ASAR6 BAC transgene integrated into mouse chromosome 3 [8]. A)
806 RNA-DNA FISH using an ASAR6 fosmid probe to detect ASAR6 RNA (green; arrows)
807 plus a mouse chromosome 3 paint probe to detect DNA (red; arrowheads). B) RNA-DNA
808 FISH using human C0T-1 DNA to detect RNA (green; arrows) plus the *ASAR6* BAC (red
809 arrowheads) to detect DNA. C-H) RNA-DNA FISH using human C0T-1 DNA as probe for
810 both RNA (middle panels, green) and DNA (top panels, red). The bottom panels show the
811 merged images. GM11687 cells were exposed to 4% 1,6-hexanediol (1,6-HD) for 20
812 minutes, washed extensively and allowed to recover for 4 hours in complete media. C)
813 Control GM11687 cells prior to 1,6-HD exposure (Untreated). D) GM11687 cells exposed
814 to 1,6-HD for 20 minutes. E) GM11687 cells exposed to 1,6-HD for 20 minutes, washed
815 extensively, and allowed to recover for 4 hours in complete media (4hr recovery). F and
816 G) GM11687 cells exposed to HD for 20 minutes, washed extensively and allowed to
817 recover for 4 hours in complete media containing Actinomycin D (4hr recovery +ActD). H)
818 Control GM11687 cells exposed to Actinomycin D for 4 hours in complete media (4hr
819 ActD).
820
821 **Figure S1. CRISPR/Cas9 deletion of the ~7kb RBPD.** A) Integrative Genomics Viewer
822 view showing the genomic location of *ASAR6-141*. The genomic locations of RNAseq
823 and eCLIP reads from HepG2 and K562 (from ENCODE) are shown. The zoomed in view
824 shows the ~7kb RBPD with the location where all of the peaks of eCLIP reads map within
825 the region (see Table S1). The location of sgRNAs that flank the ~7kb RBPD are shown.
826 The location of PCR primers (1-6) and the heterozygous SNP rs17070386 are also shown
827 (see Table S3). B) Sanger sequencing traces on PCR products generated from genomic
828 DNA using primers 5 and 6 (see Table S3). In previous studies we generated mouse
829 monochromosomal hybrid cells containing the two chromosome 6 homologs from
830 HTD114 [7], and sequencing traces from these two hybrids, contain either chromosome 6A

(CHR6A) or chromosome 6B (CHR6B) are shown below the HTD114 panel. Sequencing traces from PCR products generated from 4 heterozygous deletions, two with CHR6A deletions {D6A(7-82-29) and D6A(7-82-13)} and two with CHR6B deletions {D6B(7-18-1) and D6B(7-63-1)} are shown. C) Junction PCR (primers 1 and 4) on genomic DNA isolated from heterozygous {D6A(7-82-29), D6A(7-82-13), D6B(7-18-1) and D6B(7-63-1)} or homozygous deletions {D6B/6A-1 and D6B/6A-2} are shown. Parental HTD114 DNA was used as control. D) Internal PCR products (primers 5 and 6) on genomic DNA isolated from heterozygous {D6A(7-82-29), D6A(7-82-13), D6B(7-18-1) and D6B(7-63-1)} or homozygous deletions {D6B/6A-1 and D6B/6A-2} are shown. Parental HTD114 DNA was used as control.

Figure S2. Identification of mouse chromosomes containing the ~7kb RBPD transgene. A) DNA FISH on mouse chromosomes from clone ~7kb(+)A5. Mitotic spread showing DNA FISH using the ~7kb RBPD (magenta; arrow) and a mouse chromosome 5 BAC (RP24-107D17; red; arrowheads). B and C) DNA FISH on mouse chromosomes from clone ~7kb(+)X1. Mitotic spread showing DNA FISH using the ~7kb RBPD (magenta; arrows) and a mouse X chromosome paint (red).

Figure S3. RBP protein levels in cells expressing shRNAs. K562 or HTD114 cells were transfected with empty vector (-) or shRNA against RBPs and cell extracts were processed for Western Blots using antibodies (Table S4) as indicated: A and B) HNRNPU (green); C) UCHL5 (green); D and E) HNRNPC (green); F and I) HNRNPL (green); G and H) HNRNPM (green); J and K) KHSRP (green); L) HNRNPUL1 (green); M) HLTF (green); N) SAFB2 (green); O) PTBP1 (red); or P) HNRNPA1 (green). Tubulin (red) was used as loading control, and size markers are indicated.

Figure S4. RNA FISH on cells transfected with shRNAs that did not disrupt ASAR localization. A-D) K562 cells were transfected with empty vector (A) or shRNA expression vectors for MATR3 (B), PTBP1 (C), or PTBP2 (D). Cells were processed for RNA FISH using probes for ASAR6-141 (green; arrows) or XIST (red; arrows). E-J) HTD114 cells were transfected with empty vector (E) or shRNA expression vectors for SAFB (F), SAFB2 (G), SAFB plus SAFB2 (H), CTCF (assayed for only ASAR6 RNA) (I), or MATR3 (J). DNA was stained with DAPI, and scale bars are 10 *u*M.

Figure S5. Disruption of the chromosome territory localization of ASAR1-187 and ASAR6 RNAs following shRNA depletion of RBPs. HTD114 cells were transfected with empty vector (A) or shRNA expression vectors for HNRNPA1 (B), HNRNPC (C), HNRNPL (D), HNRNPM (E), HNRNPUL1 (F), KHSRP (G), HLTF (H), or UCHL5 (I). Cells were processed for RNA FISH using Fosmid probes (see Table S3) for ASAR1-187 (green, arrow) and ASAR6 (red, arrow). A) DNA FISH hybridization signals for chromosome 1 (CHR1 BAC DNA; magenta) and chromosome 6 (CHR6 BAC DNA; orange) are indicated by arrowheads. The brackets mark cytoplasmic regions that hybridized to both ASAR RNA FISH probes. DNA was stained with DAPI, and scale bars are 10 *u*M.

Figure S6. Replication timing in cells transfected with shRNA expression vectors. A and B) HTD114 cells were transfected with PTBP1 shRNA expression vector, exposed to BrdU for 5 hours, harvested for mitotic cells, and processed for BrdU incorporation (green) and DNA FISH using a chromosome 1 (A, red) or 6 (B, magenta) centromeric probe. Cells were exposed to BrdU for five hours, processed for BrdU incorporation using an antibody against BrdU. The ratio of BrdU incorporation in chromosome 1 and chromosome 6 homologs are shown in the bottom panels of A and B, respectively. C) HTD114 cells were transfected with shRNA expression vector for HNRNPU, exposed to BrdU for 5 hours, harvested for mitotic cells, and processed for BrdU incorporation (green) and DNA FISH using centromeric probes for chromosome 1 (red) or 6 (magenta). The ratio of BrdU incorporation in chromosome homologs for 1, 6, 12, and 18 are shown in the bottom panels. DNA was stained with DAPI, and scale bars are 10 *u*M.

Figure S7. Replication timing alterations in shRNA depleted cells. HTD114 cells were transfected with shRNA expression vectors for HNRNPA1 (A), HNRNPC (B), HNRNPL C), HNRNPM (D), HLTF (E) KHSRP (F) HNRNPU (G) or UCHL5 (H), exposed to BrdU for 5 hours, harvested for mitotic cells, and processed for BrdU incorporation (green) and DNA FISH using a chromosome 1 centromeric probe (A and G; red, arrows) or chromosome 1 paint (B, C, D, E F and H; red, arrows) plus a chromosome 6 centromeric probe (A-H; magenta, arrows). The brackets mark chromosomes with DRT/DMC. DNA was stained with DAPI, and scale bars are 10 *u*M.

Table S1. The location of significant peaks of eCLIP reads that map within ASAR and XIST genes. The location of significant, fold enrichment and log10(P value), eCLIP reads, from K562 and HepG2, that mapped within ASAR1-187, ASAR6-141, ASAR8-2.7, ASAR9-23, and XIST.

Table S2. eCLIP reads for 120 RBPs in 10 kb windows within ASAR genes. The FDR-corrected p-value of the z-score of log2-ratio between eCLiP vs control for each RBP in 10kb windows within ASAR1-187, ASAR6-141, ASAR8-2.7, and ASAR9-23, from K562 and HepG2 cells.

Table S3. Fosmids, BACS, PCR primers, and sgRNA sequences.

Table S4. shRNA and antibodies.

913 **STAR Methods**

914 *Cell culture*

915 HTD114 cells are a human *APRT* deficient cell line derived from HT1080 cells [41]. K562
916 cells were obtained from ATCC, and cultured in RPMI 1640 (Gibco) supplemented with
917 10% fetal bovine serum (Hyclone). Mouse C2C12 cells were used for the transgene
918 integration assays, transfected using Lipofectamine 2000 (Invitrogen) according to the
919 manufacturer's recommendations, and clones containing transgene integrations were
920 isolated following selection in media containing G418. All cells were grown in DMEM
921 (Gibco) supplemented with 10% fetal bovine serum (Hyclone), and were grown in a
922 humidified incubator at 37°C in a 5% carbon dioxide atmosphere.

923

924 *eCLIP analysis*

925 eCLIP data was obtained from [42]**.** Given that non-coding genes and TLs are expressed
926 at a lower level than coding genes, a sensitive filtering approach was used as
927 recommended by the authors [42]. We filtered out peaks containing an eCLIP peak p-value
928 greater than p=0.05, and filtered out peaks containing a fold enrichment value less than
929 two.

930

931 *Identification of TL*

932 Nuclear-enriched, strand-specific, ribo-minus, total-RNA sequencing libraries were first
933 aligned to the hg19 reference genome using default parameters with STAR [43]. Next
934 SAMtools [44] was used to remove duplicate and low quality (<=MAPQ20) reads. TLs were
935 defined using a strategy of sequential merging of strand-specific, contiguous intergenic

936 reads, as performed in [6]. Utilizing strand-specific reads, stranded reads separated by
937 1,000 bp or less were merged to create contigs, and the contigs merged again while
938 allowing for gaps of 7 kb to allow for regions that are not uniquely mappable due to
939 presence of full-length LINE elements. TL were then classified above a minimum cutoff
940 length of 50 kb of strand specific, contiguous expression.
941
942 *shRNA depletion of RBPs*
943 Using Lipofectamine 2000 (Invitrogen), according to the manufacturer's
944 recommendations, we co-transfected HTD114 cells with plasmids encoding puromycin
945 resistance (PGK-PURO) and shRNAs against 14 different RBPs (Table S4). 24h after
946 transfection, cells were plated in media containing 10 ug/ml puromycin (Millipore/Sigma),
947 and 24h-48h following puromycin selection cells were processed for Western blot, RNA-
948 DNA FISH or for replication timing assays (see below).
949
950 *Western blot analysis.*
951 Cells were pelleted, rinsed once in PBS, and lysed by resuspension in RIPA Solubilization
952 Buffer (25 mM Tris-HCl pH 7.6, 150 mM NaCl, 5 mM EDTA,1% NP-40 or 1% Triton X-
953 100, 1% sodium deoxycholate, 0.1% SDS). Protein concentration was determined via the
954 Qubit Protein BR Assay kit (Invitrogen, A50669) on a Qubit 4 Fluorometer. Lysates from
955 HTD114 (20 μg) or K562 (25 μg) cell lines in 1X Laemmli Sample Buffer (Bio-Rad, 161-
956 0737) with 5% β-mercaptoethanol were loaded onto 10% Mini-PROTEAN TGX Precast
957 Tris-Glycine-SDS polyacrylamide gels, and run in 1X SDS PAGE running buffer (Bio-Rad,
958 161-0732) at 100 Volts for 1.25 hours. Proteins were transferred to either NitroBind

959 nitrocellulose (GE, EP4HY00010) or Immobilon-FL PVDF (Millipore, IPFL00010)
960 membranes in Tris-Glycine transfer buffer (25 mM Tris, 192 mM glycine, 20% methanol
961 pH 8.3) at 100 V for one hour.
962 For protein detection, membranes were blocked for one hour in 50% AquaBlock (Arlington
963 Scientific, PP82P-500-QT-1582) in PBS (AquaBlock-P) and probed with specific
964 antibodies (Table S4) in AquaBlock-P with 0.1% Tween 20 (AquaBlock-PT) at 4 °C
965 overnight. The membranes were subjected to four 5-minutes washes in PBS with 0.1%
966 Tween 20 (PBS-T) at room temperature. Membranes were then incubated with secondary
967 antibodies in AquaBlock-PT for one hour at room temperature, and subjected to four
968 washes in PBS-T as described above. Antibody labeling was detected using an Azure
969 Sapphire Biomolecular Imager.
970
971 *Immunofluorescence:*
972 Cells were allowed to attach to poly-L lysing coated glass slides for 2 hours. Cells were
973 fixed with 4% paraformaldehyde in PBS pH 7.4 for 10 min at room temperature, then
974 washed 3X with ice-cold PBS. Cells were Permeabilized for 10 min with PBS containing
975 either 0.1% Triton X-100 (PBST), and washed 3X with PBS at room temperature. Prior to
976 antibody addition, slides were incubated for 30 minutes with 10% serum from the species
977 the secondary antibody was raised in. Slides were incubated in diluted primary antibody
978 in 1% BSA in PBST in a humidified chamber overnight at 4°C. Slides were washed three
979 times in PBS, 5 min each wash. Slides were incubated with secondary antibody in 1%
980 BSA for 1 h at room temperature in the dark. Slides were wash three times with PBS for
981 5 min each in the dark.

982

983 *CRISPR/Cas9 engineering*

984 Using Lipofectamine 2000 (Invitrogen), according to the manufacturer's
985 recommendations, we co-transfected HTD114 cells with plasmids encoding GFP,
986 sgRNAs and Cas9 endonuclease (Origene). Each plasmid encoded sgRNA was designed
987 to bind at the indicated locations (Fig. S1). 48h after transfection, cells were plated at
988 clonal density and allowed to expand for 2-3 weeks. The presence of deletions was
989 identified by PCR using the primers described in Figure S1. The single cell colonies that
990 grew were analyzed for heterozygous deletions by PCR (Fig. S1). We used retention of a
991 heterozygous SNP to identify the disrupted allele, and homozygosity at the SNP confirmed
992 that cell clones were homogenous.

993

994 *PCR analysis*

995 Genomic DNA was isolated from tissue culture cells using TRIZOL Reagent (Invitrogen).
996 PCR was performed in a 12.5μL volume using 50-100ng of genomic DNA, 1x Standard
997 Taq Buffer (New England Biolabs, Inc.), 200μM each deoxynucleotide triphosphates,
998 0.2μM of each primer, and 3 units of Taq DNA Polymerase (New England Biolabs, Inc.)
999 under the following reaction conditions: 95°C for 2 minutes, followed by 30-40 cycles of
1000 95°C for 30 seconds, 55-62°C for 45 seconds, and 72°C for 1 minute, with a final
1001 extension time of 10 minutes at 72°C. PCR products were separated on 1% agarose gels,
1002 stained with ethidium bromide, and photographed under ultraviolet light illumination.
1003 Sequencing of PCR products was carried out at the Vollum Institute DNA Sequencing
1004 Core facility.

1005

1006 *DNA FISH*

1007 Mitotic chromosome spreads were prepared as described previously [34]. After RNase
1008 (100µg/ml) treatment for 1h at 37°C, slides were washed in 2XSSC and dehydrated in an
1009 ethanol series and allowed to air dry. Chromosomal DNA on the slides was denatured at
1010 75°C for 3 minutes in 70% formamide/2XSSC, followed by dehydration in an ice-cold
1011 ethanol series and allowed to air dry. BAC and Fosmid DNAs were labeled using nick
1012 translation (Vysis, Abbott Laboratories) with Spectrum Orange-dUTP, Spectrum Aqua-
1013 dUTP or Spectrum Green-dUTP (Vysis). Final probe concentrations varied from 40-60
1014 ng/µl. Centromeric probe cocktails (Vysis) and/or whole chromosome paint probes
1015 (Metasystems) plus BAC or Fosmid DNAs were denatured at 75°C for 10 minutes and
1016 prehybridized at 37°C for 10 minutes. Probes were applied to denatured slides and
1017 incubated overnight at 37°C. Post-hybridization washes consisted of one 3-minute wash
1018 in 50% formamide/2XSSC at 40°C followed by one 2-minute rinse in PN (0.1M Na_2HPO_4,
1019 pH 8.0/2.5% Nonidet NP-40) buffer at RT. Coverslips were mounted with Prolong Gold
1020 antifade plus DAPI (Invitrogen) and viewed under UV fluorescence (Olympus).

1021

1022 *RNA-DNA FISH*

1023 Cells were plated on Poly-L-Lysine coated (Millipore Singa) glass microscope slides at
1024 ~50% confluence and incubated for 4 hours in complete media in a 37°C humidified CO_2
1025 incubator. Slides were rinsed 1X with sterile RNase free PBS. Cell Extraction was carried
1026 out using ice cold solutions as follows: Slides were incubated for 30 seconds in CSK buffer
1027 (100mM NaCl/300mM sucrose/3mM $MgCl_2$/10mM PIPES, pH 6.8), 10 minutes in CSK

1028 buffer/0.1% Triton X-100, followed by 30 seconds in CSK buffer. Cells were then fixed in
1029 4% paraformaldehyde in PBS for 10 minutes and stored in 70% EtOH at -20°C until use.
1030 Just prior to RNA FISH, slides were dehydrated through an EtOH series and allowed to
1031 air dry. Denatured probes were prehybridized at 37°C for 10 min, applied to non-
1032 denatured slides and hybridized at 37°C for 14-16 hours. Post-hybridization washes
1033 consisted of one 3-minute wash in 50% formamide/2XSSC at 40°C followed by one 2-
1034 minute rinse in 2XSSC/0.1% TX-100 for 1 minute at RT. Slides were then fixed in 4%
1035 paraformaldehyde in PBS for 5 minutes at RT, and briefly rinsed in 2XSSC/0.1% TX-100
1036 at RT. Coverslips were mounted with Prolong Gold antifade plus DAPI (Invitrogen) and
1037 slides were viewed under UV fluorescence (Olympus). Z-stack images were generated
1038 using a Cytovision workstation. After capturing RNA FISH signals, the coverslips were
1039 removed, the slides were dehydrated in an ethanol series, and then processed for DNA
1040 FISH, beginning with the RNase treatment step, as described above.
1041
1042 *Chromosome replication timing assay*
1043 The BrdU replication timing assay was performed as described previously on
1044 exponentially dividing cultures and asynchronously growing cells [35]. Mitotic chromosome
1045 spreads were prepared and DNA FISH was performed as described above. The
1046 incorporated BrdU was then detected using a FITC-labeled anti-BrdU antibody (Roche).
1047 Coverslips were mounted with Prolong Gold antifade plus DAPI (Invitrogen), and viewed
1048 under UV fluorescence. All images were captured with an Olympus BX Fluorescent
1049 Microscope using a 100X objective, automatic filter-wheel and Cytovision workstation.
1050 Individual chromosomes were identified with either chromosome-specific paints,

1051 centromeric probes, BACs or by inverted DAPI staining. Utilizing the Cytovision
1052 workstation, each chromosome was isolated from the metaphase spread and a line drawn
1053 along the middle of the entire length of the chromosome. The Cytovision software was
1054 used to calculate the pixel area and intensity along each chromosome for each
1055 fluorochrome occupied by the DAPI and BrdU (FITC) signals. The total amount of
1056 fluorescent signal in each chromosome was calculated by multiplying the average pixel
1057 intensity by the area occupied by those pixels. The BrdU incorporation into human
1058 chromosomes containing CRISPR/Cas9 modifications was calculated by dividing the total
1059 incorporation into the chromosome with the deleted chromosome divided by the BrdU
1060 incorporation into the non-deleted chromosome within the same cell. Boxplots were
1061 generated from data collected from 8-12 cells per clone or treatment group. Differences
1062 in measurements were tested across categorical groupings by using the Kruskal-Wallis
1063 test [40] and listed as P-values for the corresponding plots.
1064
1065

RESOURCE AVAILABILITY

Further information and requests for resources and reagents should be directed to and will be fulfilled by the lead contact, Mathew Thayer (thayerm@ohsu.edu)

Materials availability statement

All reagents generated in this study will be made freely available upon request.

Acknowledgments:

M.J.T. was supported by NIH NIGMS (R01GM114162 and R01GM130703).

M.B.H was supported by NIH NCI 4K00CA245677-03

Author contributions:

Declaration of interests

The authors declare no competing interests.

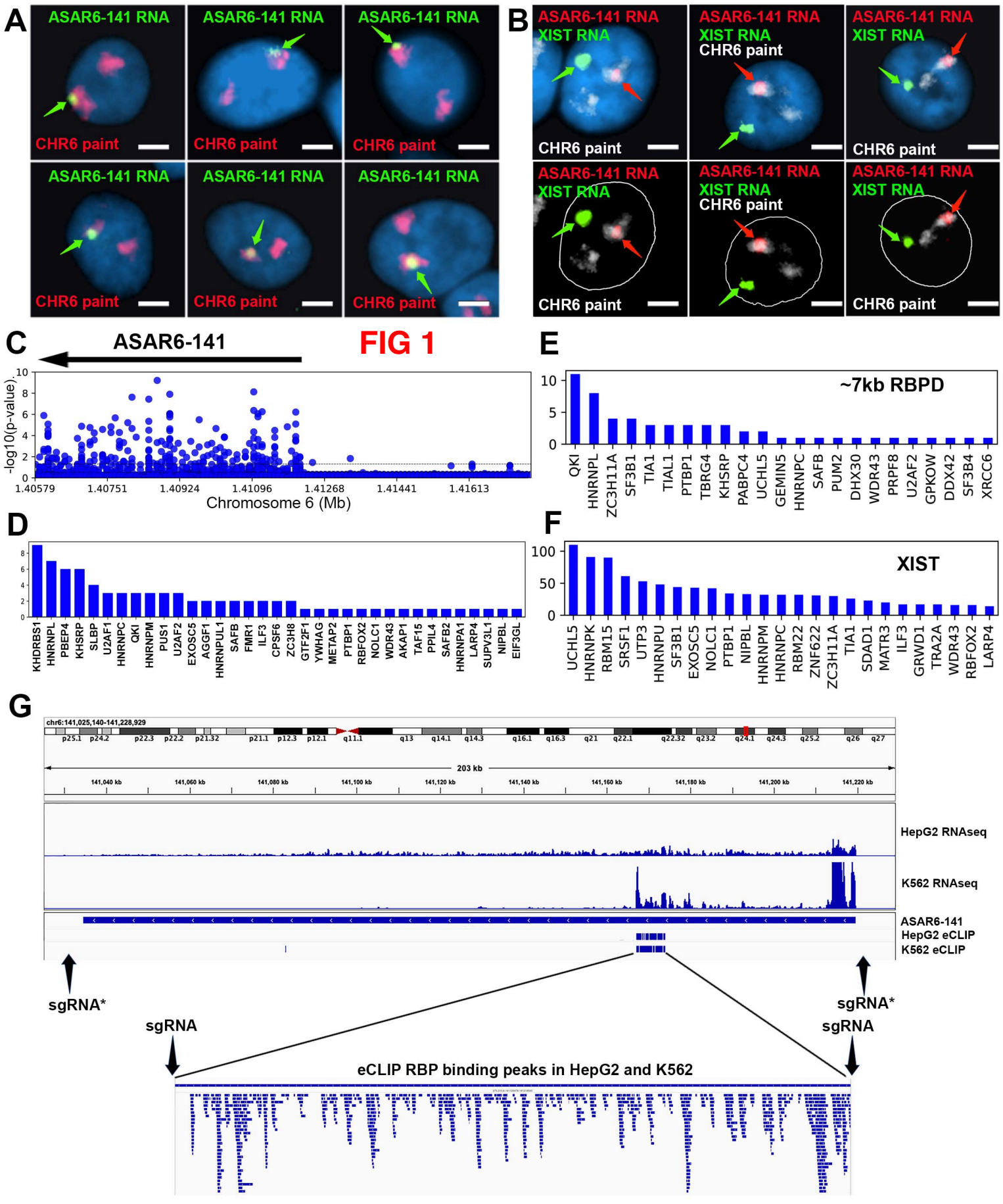
A
ASAR6-141 RNA
CHR6 paint
B
ASAR6-141 RNA
XIST RNA
CHR6 paint
C
ASAR6-141
FIG 1
-log10(p-value)
Chromosome 6 (Mb)
1.40579
1.40751
1.40924
1.41096
1.41268
1.41441
1.41613
D
KHDRBS1
HNRNPL
PBEP4
KHSRP
SLBP
U2AF1
HNRNPC
QKI
HNRNPM
PUS1
U2AF2
EXOSC5
AGGF1
HNRNPUL1
SAFB
FMR1
ILF3
CPSF6
ZC3H8
GTF2F1
YWHAG
METAP2
PTBP1
RBFOX2
NOLC1
WDR43
AKAP1
TAF15
PPIL4
SAFB2
HNRNPA1
LARP4
SUPV3L1
NIPBL
EIF3GL
E
~7kb RBPD
QKI
HNRNPL
ZC3H11A
SF3B1
TIA1
TIAL1
PTBP1
TBRG4
KHSRP
PABPC4
UCHL5
GEMIN5
HNRNPC
SAFB
PUM2
DHX30
WDR43
PRPF8
U2AF2
GPKOW
DDX42
SF3B4
XRCC6
F
XIST
UCHL5
HNRNPK
RBM15
SRSF1
UTP3
HNRNPU
SF3B1
EXOSC5
NOLC1
PTBP1
NIPBL
HNRNPM
HNRNPC
RBM22
ZNF622
ZC3H11A
TIA1
SDAD1
MATR3
ILF3
GRWD1
TRA2A
WDR43
RBFOX2
LARP4
G
chr6:141,025,140-141,228,929
203 kb
HepG2 RNAseq
K562 RNAseq
ASAR6-141
HepG2 eCLIP
K562 eCLIP
sgRNA*
sgRNA
sgRNA*
sgRNA
eCLIP RBP binding peaks in HepG2 and K562

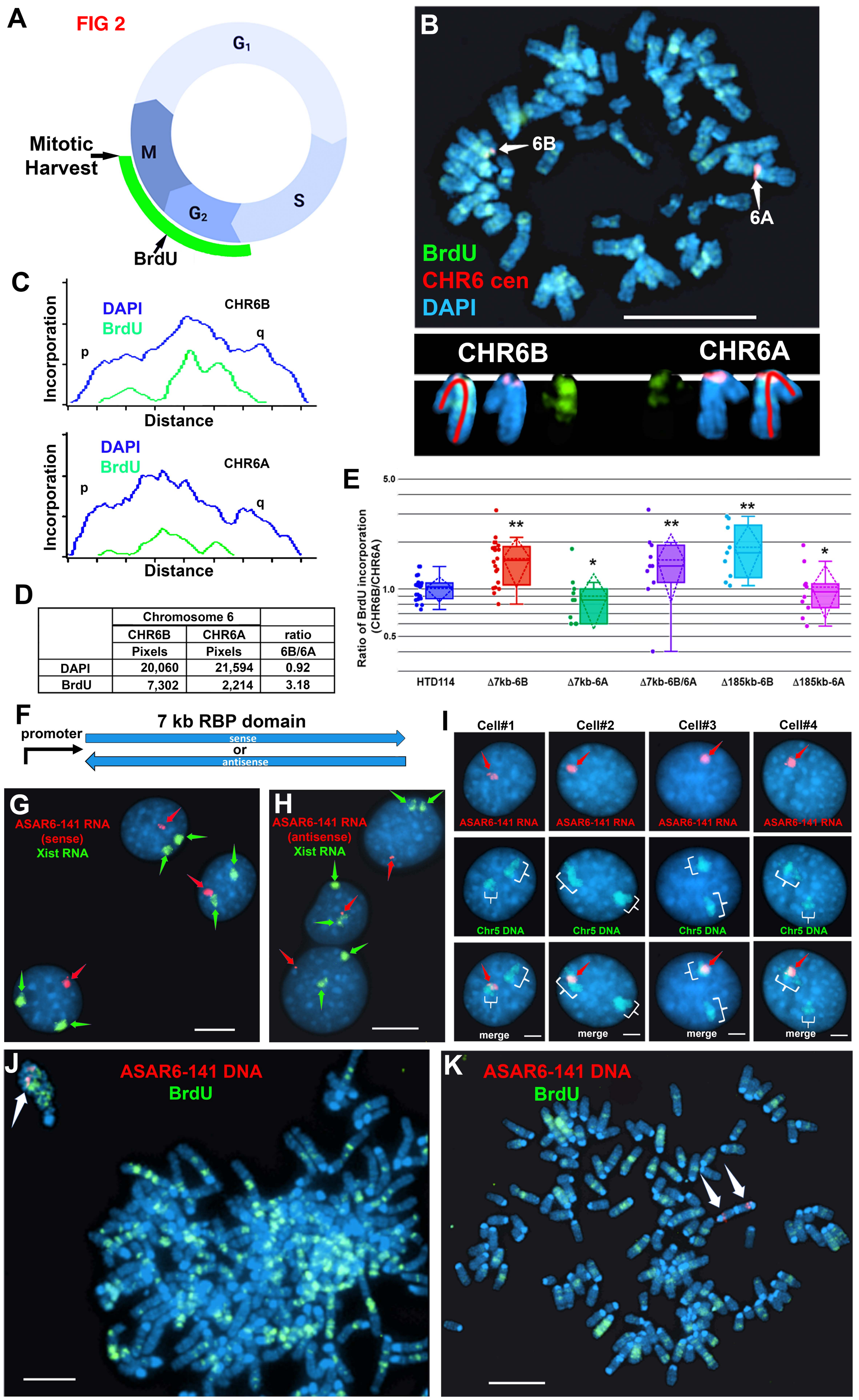

	Chromosome 6		
	CHR6B	CHR6A	ratio
	Pixels	Pixels	6B/6A
DAPI	20,060	21,594	0.92
BrdU	7,302	2,214	3.18

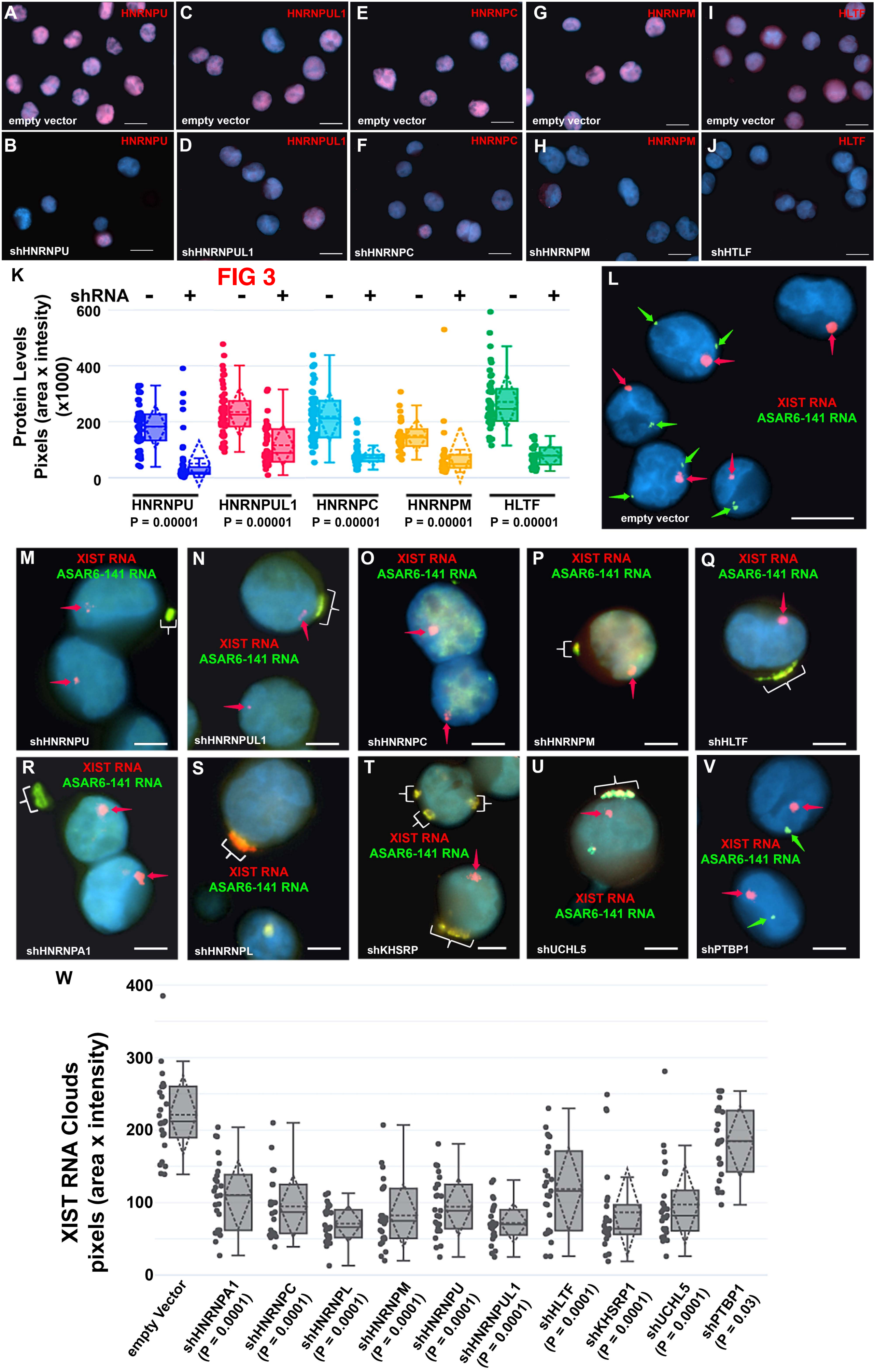
FIG 3
A
HNRNPU
empty vector
B
HNRNPU
shHNRNPU
C
HNRNPUL1
empty vector
D
HNRNPUL1
shHNRNPUL1
E
HNRNPC
empty vector
F
HNRNPC
shHNRNPC
G
HNRNPM
empty vector
H
HNRNPM
shHNRNPM
I
HLTF
empty vector
J
HLTF
shHTLF
K
shRNA - + - + - + - + - +
Protein Levels
Pixels (area x intesity)
(x1000)
600
400
200
0
HNRNPU
P = 0.00001
HNRNPUL1
P = 0.00001
HNRNPC
P = 0.00001
HNRNPM
P = 0.00001
HLTF
P = 0.00001
L
XIST RNA
ASAR6-141 RNA
empty vector
M
XIST RNA
ASAR6-141 RNA
shHNRNPU
N
XIST RNA
ASAR6-141 RNA
shHNRNPUL1
O
XIST RNA
ASAR6-141 RNA
shHNRNPC
P
XIST RNA
ASAR6-141 RNA
shHNRNPM
Q
XIST RNA
ASAR6-141 RNA
shHLTF
R
XIST RNA
ASAR6-141 RNA
shHNRNPA1
S
XIST RNA
ASAR6-141 RNA
shHNRNPL
T
XIST RNA
ASAR6-141 RNA
shKHSRP
U
XIST RNA
ASAR6-141 RNA
shUCHL5
V
XIST RNA
ASAR6-141 RNA
shPTBP1
W
XIST RNA Clouds
pixels (area x intensity)
400
300
200
100
0
empty Vector
shHNRNPA1 (P = 0.0001)
shHNRNPC (P = 0.0001)
shHNRNPL (P = 0.0001)
shHNRNPM (P = 0.0001)
shHNRNPU (P = 0.0001)
shHNRNPUL1 (P = 0.0001)
shHLTF (P = 0.0001)
shKHSRP1 (P = 0.0001)
shUCHL5 (P = 0.0001)
shPTBP1 (P = 0.03)

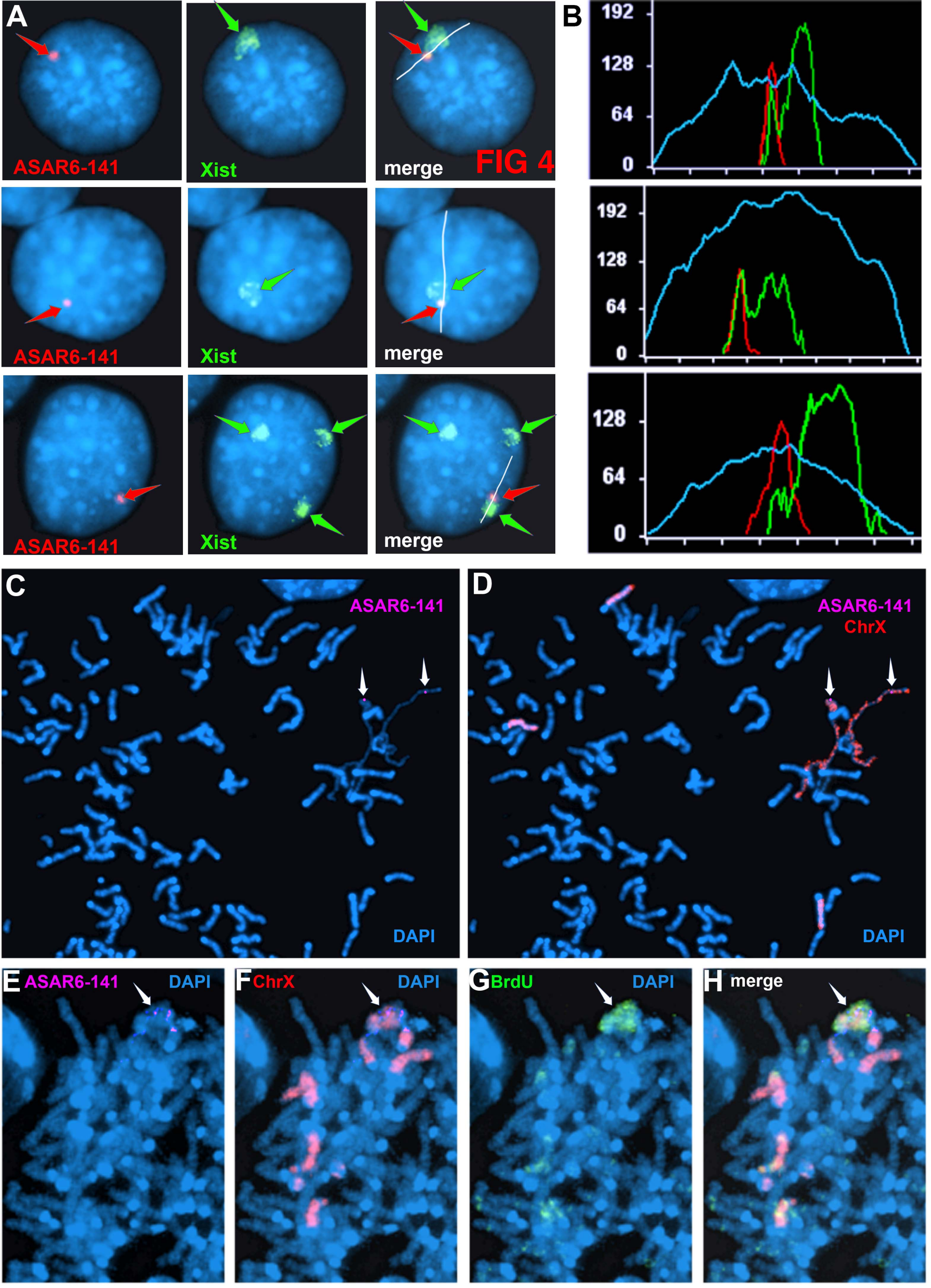
A
ASAR6-141
Xist
merge
FIG 4
B
192
128
64
0
C
ASAR6-141
DAPI
D
ASAR6-141
ChrX
DAPI
E ASAR6-141
DAPI
F ChrX
DAPI
G BrdU
DAPI
H merge

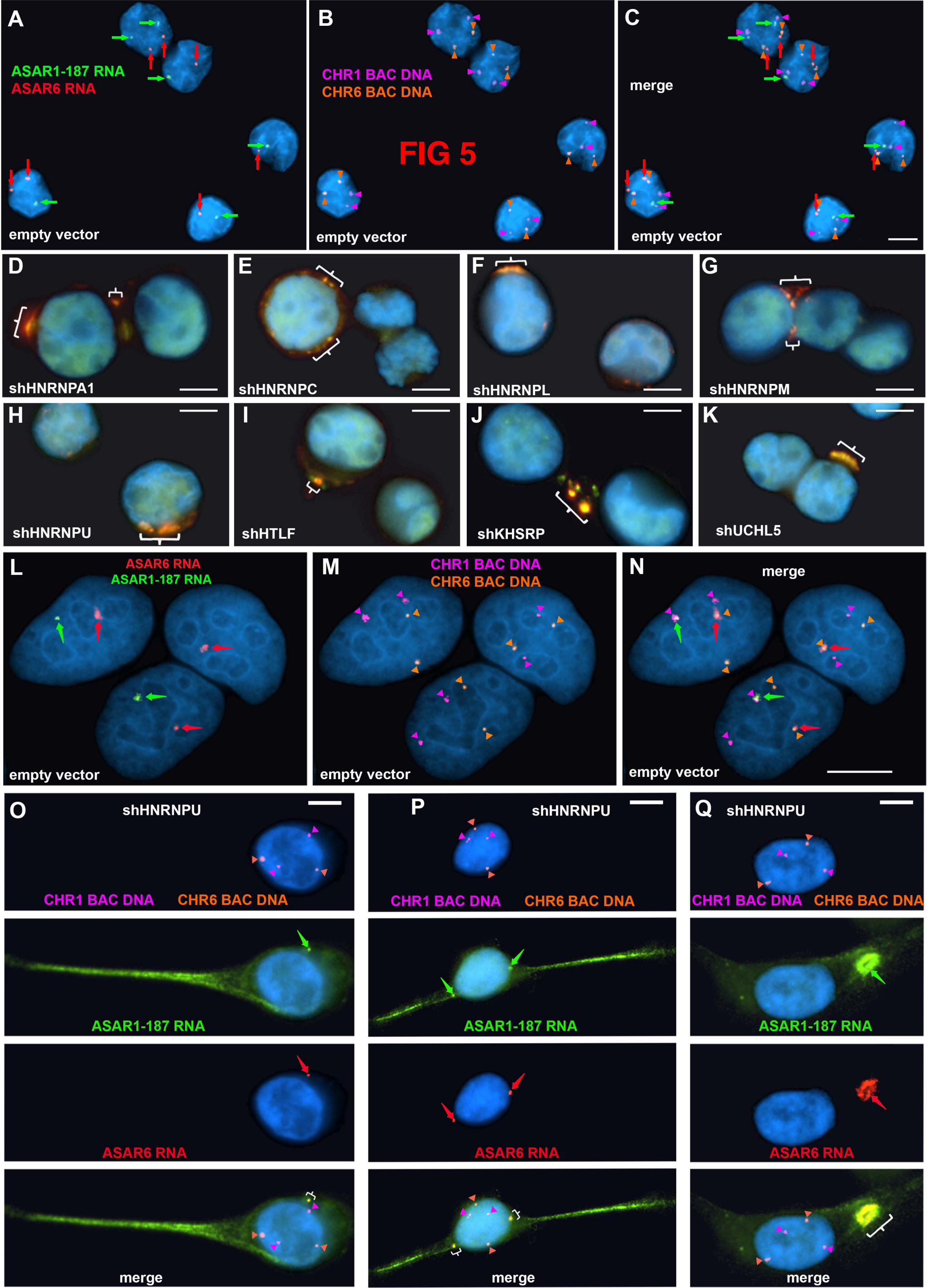
A
ASAR1-187 RNA
ASAR6 RNA
empty vector
B
CHR1 BAC DNA
CHR6 BAC DNA
empty vector
C
merge
empty vector
FIG 5
D
shHNRNPA1
E
shHNRNPC
F
shHNRNPL
G
shHNRNPM
H
shHNRNPU
I
shHTLF
J
shKHSRP
K
shUCHL5
L
ASAR6 RNA
ASAR1-187 RNA
empty vector
M
CHR1 BAC DNA
CHR6 BAC DNA
empty vector
N
merge
empty vector
O
shHNRNPU
CHR1 BAC DNA
CHR6 BAC DNA
ASAR1-187 RNA
ASAR6 RNA
merge
P
shHNRNPU
CHR1 BAC DNA
CHR6 BAC DNA
ASAR1-187 RNA
ASAR6 RNA
merge
Q
shHNRNPU
CHR1 BAC DNA
CHR6 BAC DNA
ASAR1-187 RNA
ASAR6 RNA
merge

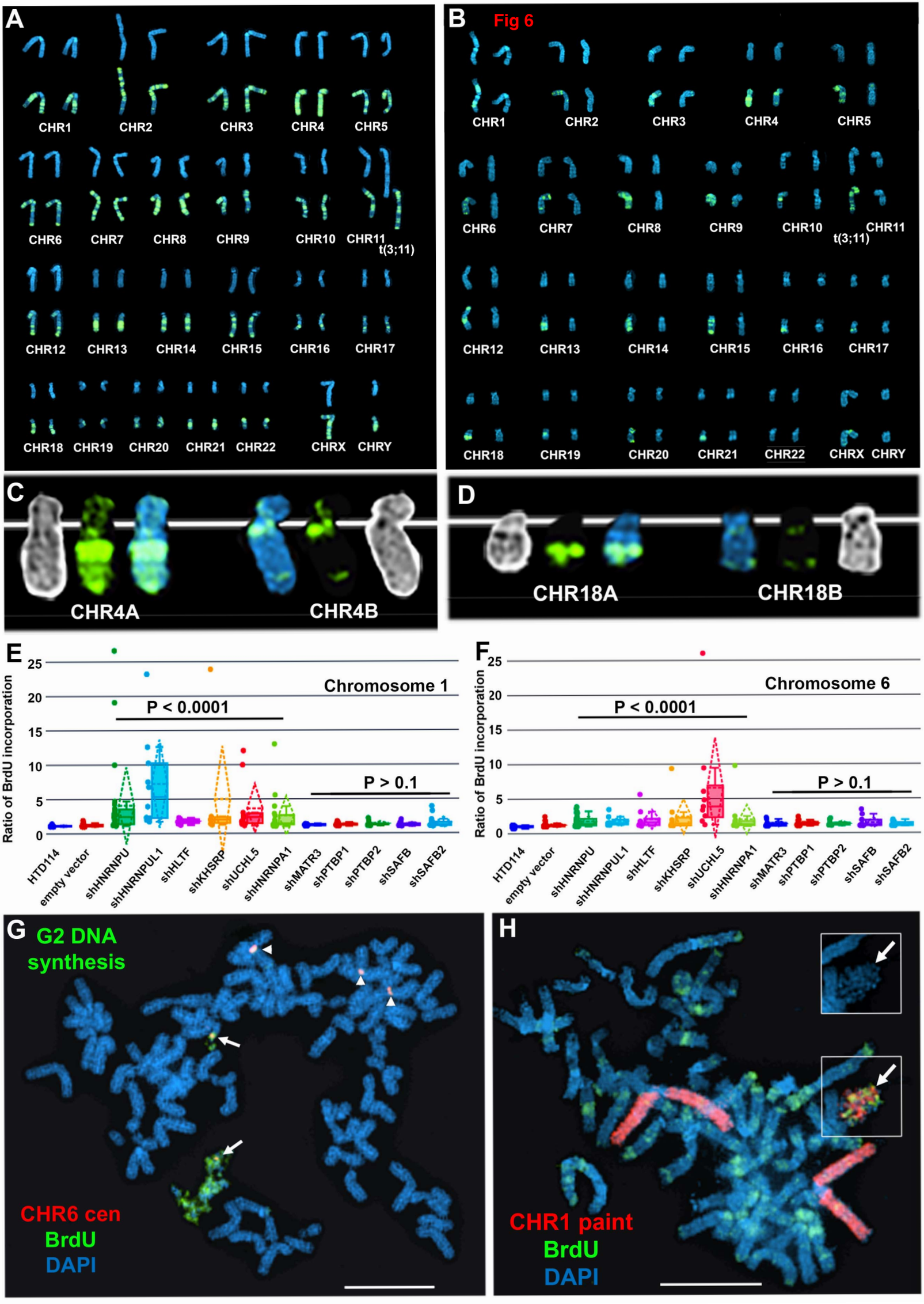
A
CHR1
CHR2
CHR3
CHR4
CHR5
CHR6
CHR7
CHR8
CHR9
CHR10
CHR11
t(3;11)
CHR12
CHR13
CHR14
CHR15
CHR16
CHR17
CHR18
CHR19
CHR20
CHR21
CHR22
CHRX
CHRY
B
Fig 6
CHR1
CHR2
CHR3
CHR4
CHR5
CHR6
CHR7
CHR8
CHR9
CHR10
CHR11
t(3;11)
CHR12
CHR13
CHR14
CHR15
CHR16
CHR17
CHR18
CHR19
CHR20
CHR21
CHR22
CHRX
CHRY
C
CHR4A
CHR4B
D
CHR18A
CHR18B
E
Chromosome 1
P < 0.0001
P > 0.1
Ratio of BrdU incorporation
0
5
10
15
20
25
HTD114
empty vector
shHNRNPU
shHNRNPUL1
shHLTF
shKHSRP
shUCHL5
shHNRNPA1
shMATR3
shPTBP1
shPTBP2
shSAFB
shSAFB2
F
Chromosome 6
P < 0.0001
P > 0.1
Ratio of BrdU incorporation
0
5
10
15
20
25
HTD114
empty vector
shHNRNPU
shHNRNPUL1
shHLTF
shKHSRP
shUCHL5
shHNRNPA1
shMATR3
shPTBP1
shPTBP2
shSAFB
shSAFB2
G
G2 DNA synthesis
CHR6 cen
BrdU
DAPI
H
CHR1 paint
BrdU
DAPI

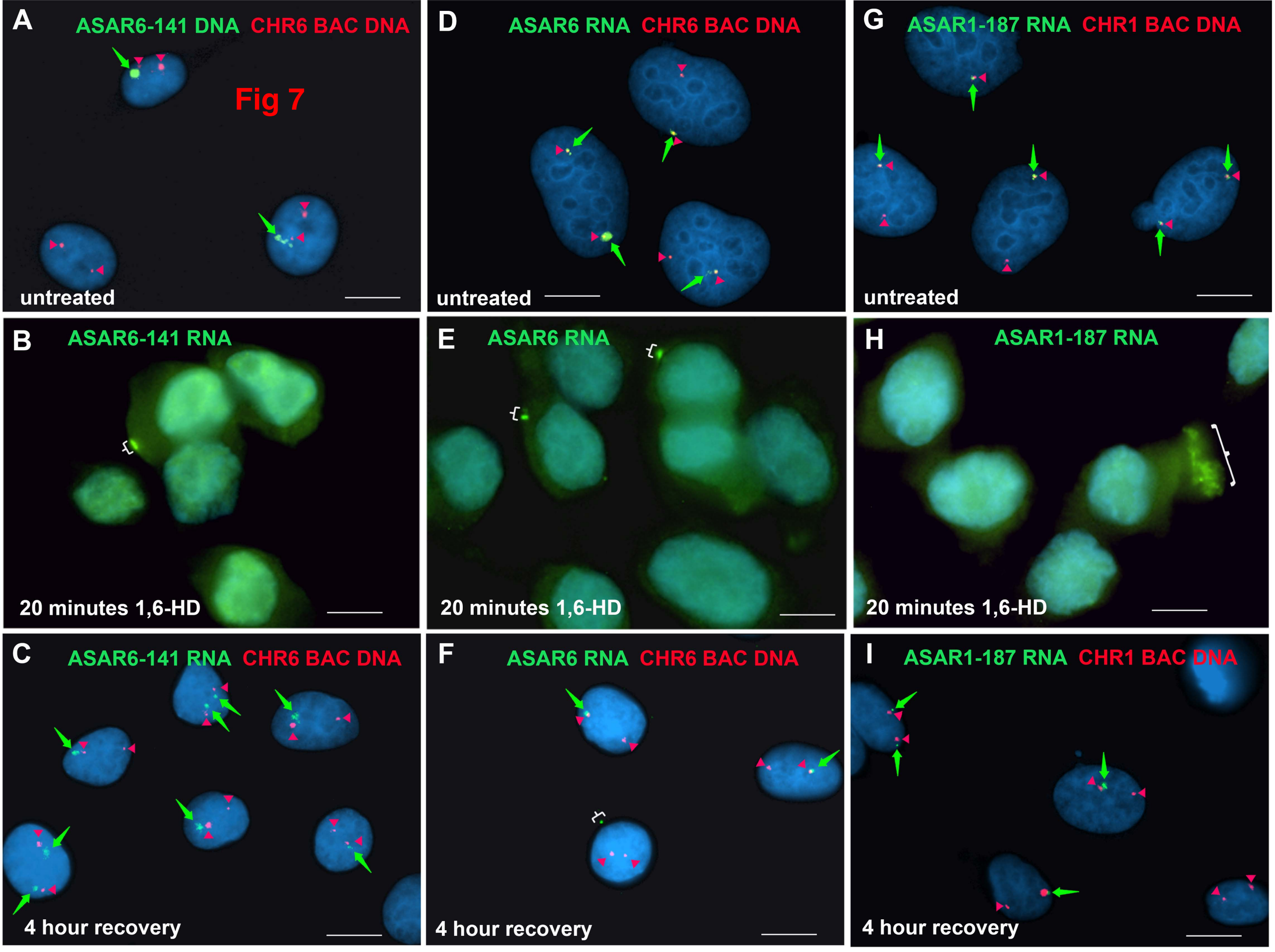
A
ASAR6-141 DNA
CHR6 BAC DNA
Fig 7
untreated
D
ASAR6 RNA
CHR6 BAC DNA
untreated
G
ASAR1-187 RNA
CHR1 BAC DNA
untreated
B
ASAR6-141 RNA
20 minutes 1,6-HD
E
ASAR6 RNA
20 minutes 1,6-HD
H
ASAR1-187 RNA
20 minutes 1,6-HD
C
ASAR6-141 RNA
CHR6 BAC DNA
4 hour recovery
F
ASAR6 RNA
CHR6 BAC DNA
4 hour recovery
I
ASAR1-187 RNA
CHR1 BAC DNA
4 hour recovery

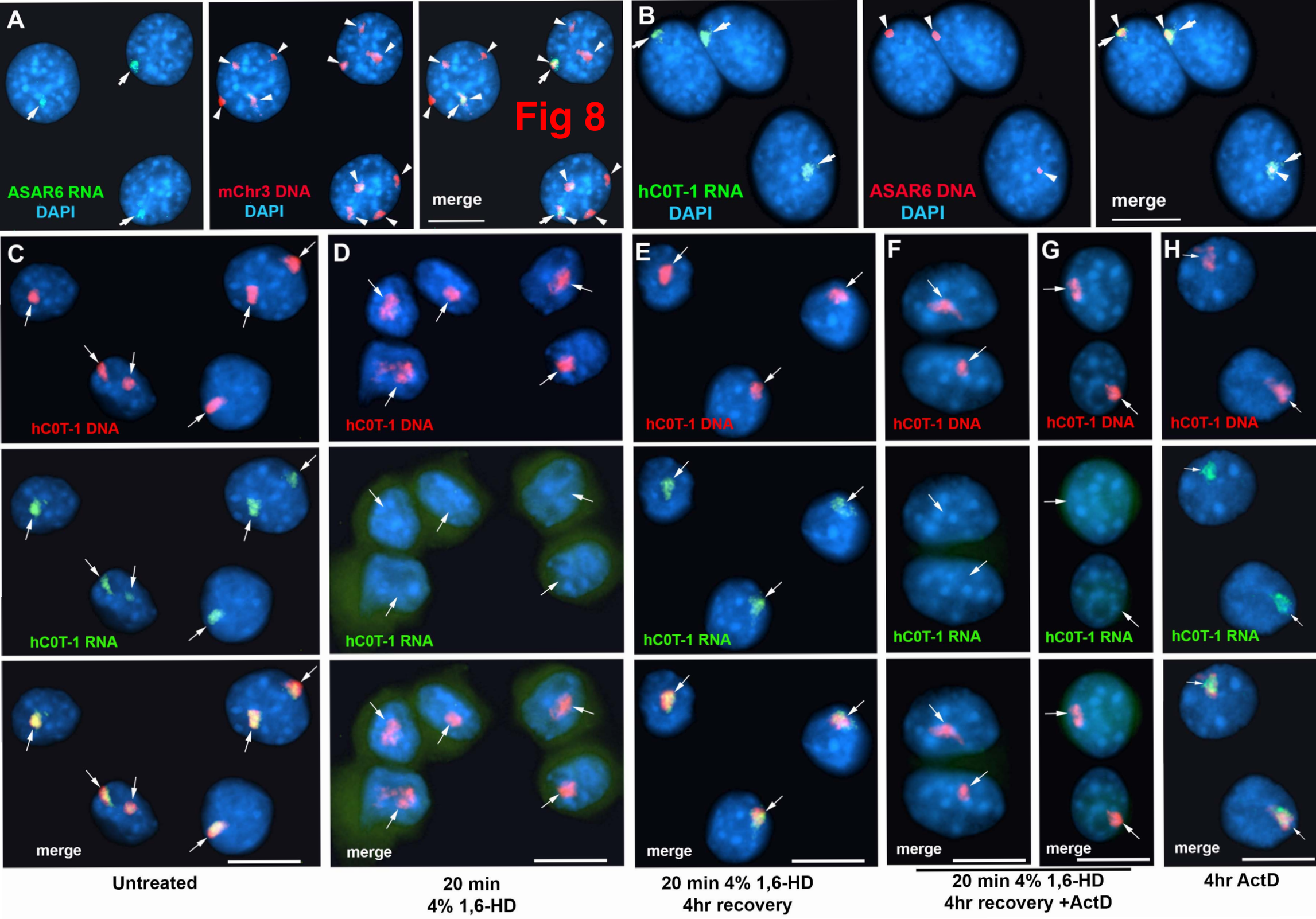
Fig 8
A
ASAR6 RNA
DAPI
mChr3 DNA
DAPI
merge
B
hC0T-1 RNA
DAPI
ASAR6 DNA
DAPI
merge
C
D
E
F
G
H
hC0T-1 DNA
hC0T-1 RNA
merge
Untreated
20 min
4% 1,6-HD
20 min 4% 1,6-HD
4hr recovery
20 min 4% 1,6-HD
4hr recovery +ActD
4hr ActD

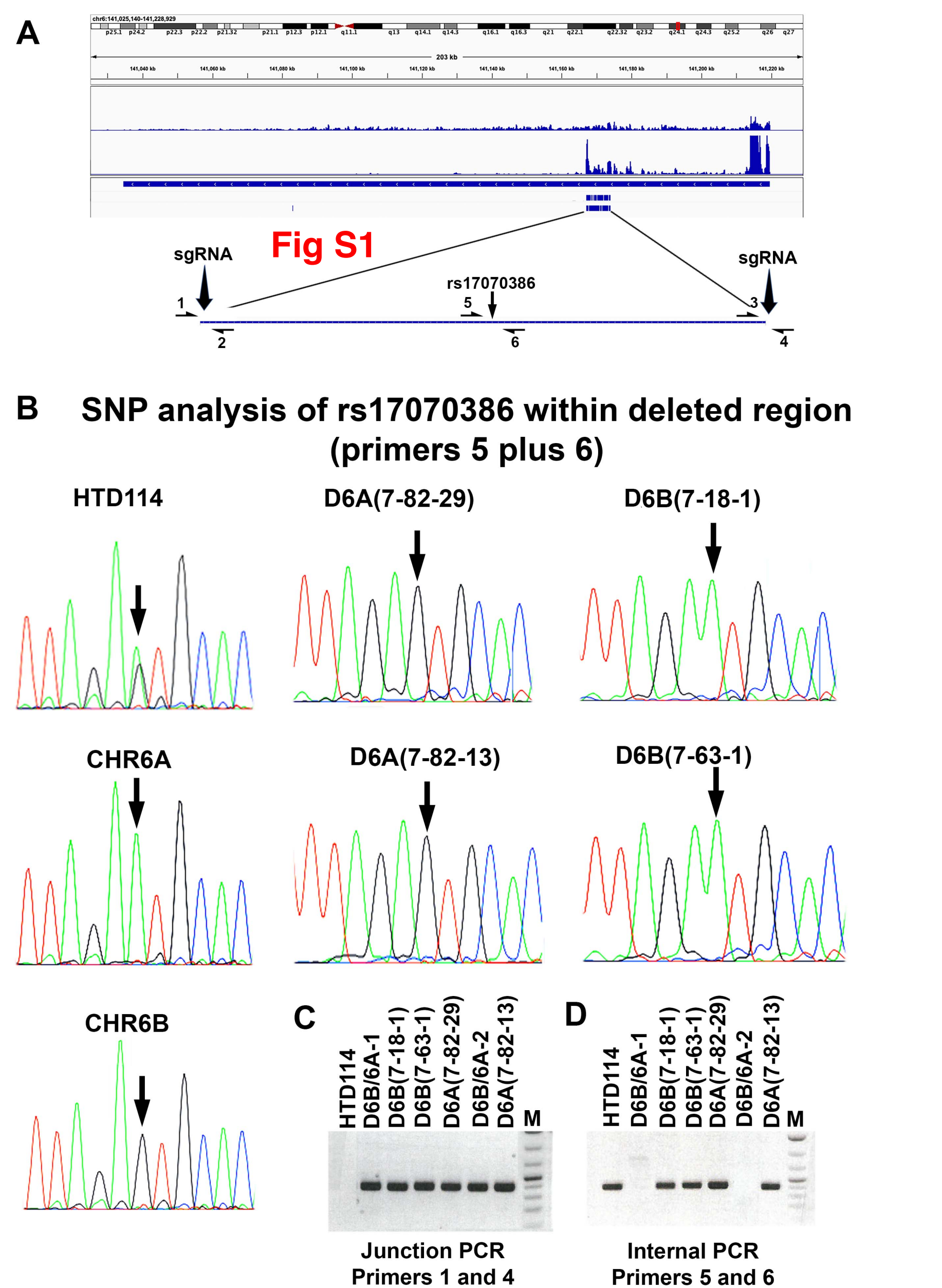
A
chr6:141,025,140-141,228,929
203 kb
Fig S1
sgRNA
sgRNA
rs17070386
1
2
5
6
3
4
B
SNP analysis of rs17070386 within deleted region
(primers 5 plus 6)
HTD114
D6A(7-82-29)
D6B(7-18-1)
CHR6A
D6A(7-82-13)
D6B(7-63-1)
CHR6B
C
HTD114
D6B/6A-1
D6B(7-18-1)
D6B(7-63-1)
D6A(7-82-29)
D6B/6A-2
D6A(7-82-13)
M
Junction PCR
Primers 1 and 4
D
HTD114
D6B/6A-1
D6B(7-18-1)
D6B(7-63-1)
D6A(7-82-29)
D6B/6A-2
D6A(7-82-13)
M
Internal PCR
Primers 5 and 6

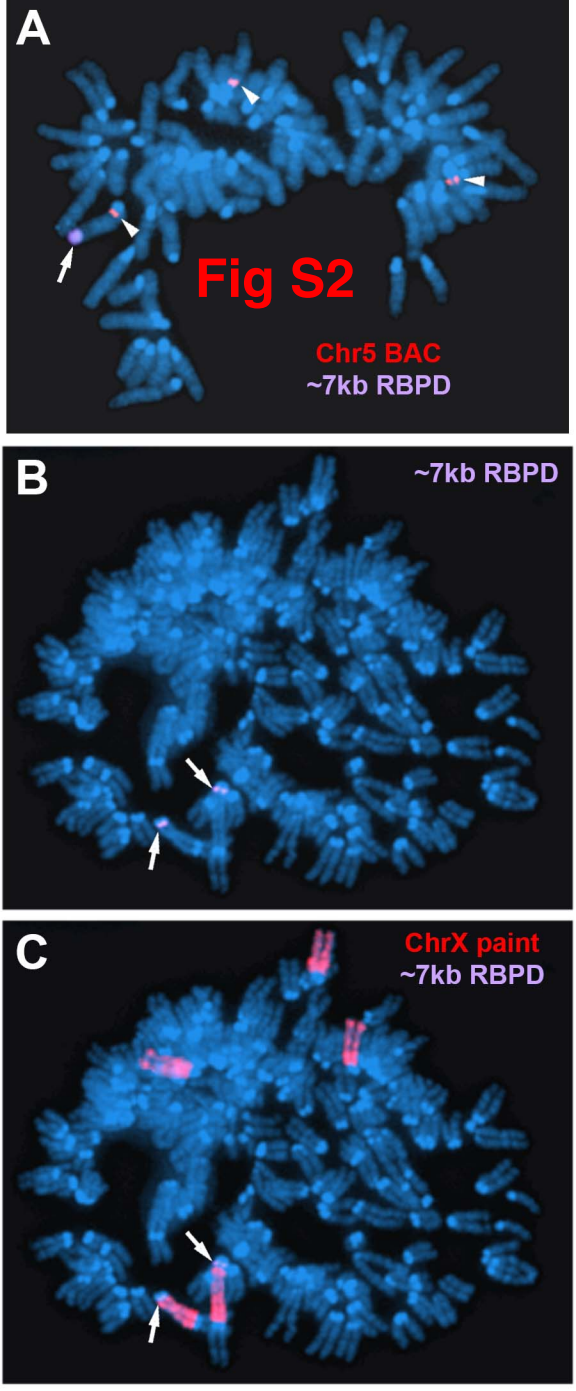
A
Fig S2
Chr5 BAC
~7kb RBPD
B
~7kb RBPD
C
ChrX paint
~7kb RBPD

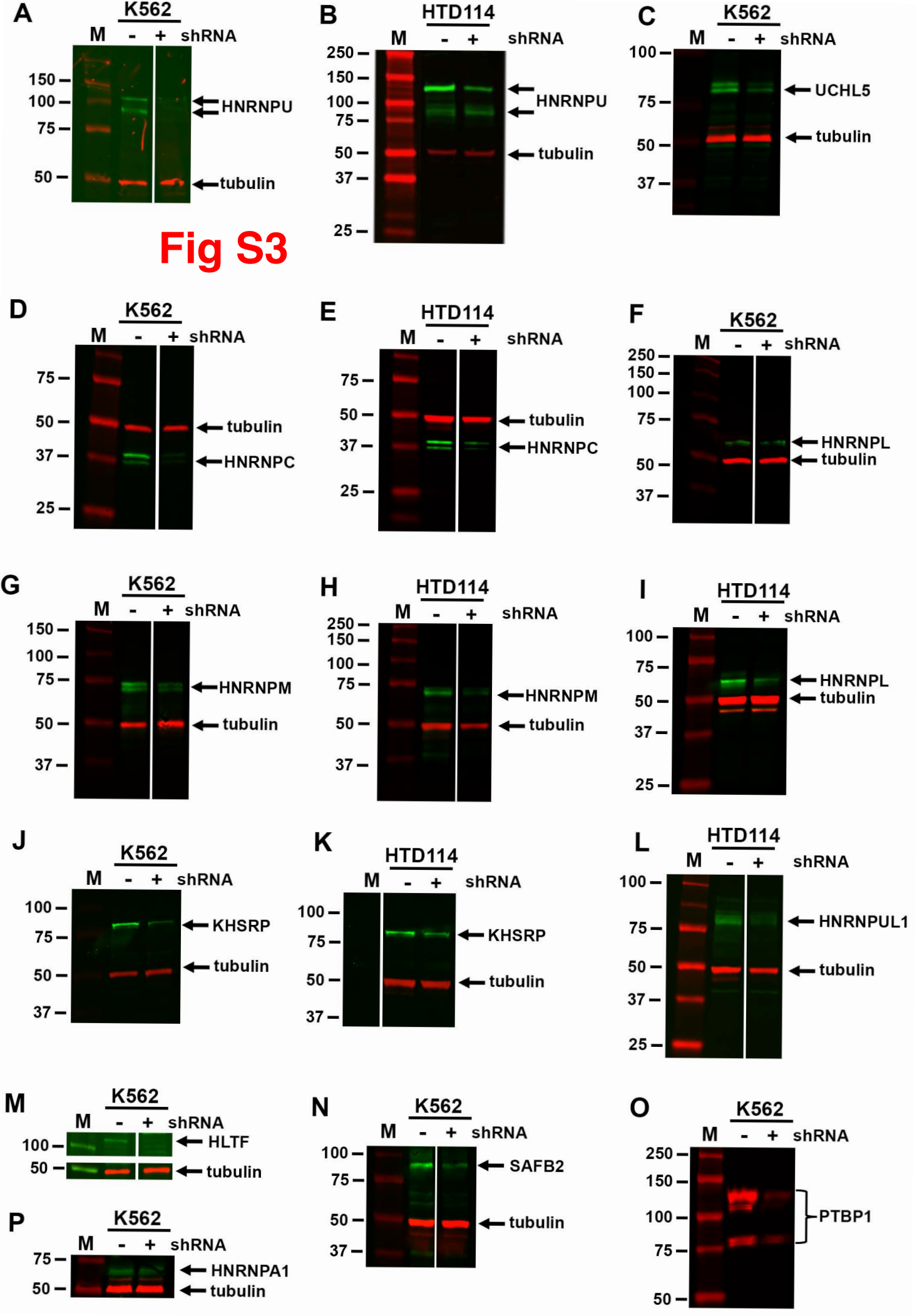
A
K562
M - + shRNA
150
100
75
50
HNRNPU
tubulin
B
HTD114
M - + shRNA
250
150
100
75
50
37
25
HNRNPU
tubulin
C
K562
M - + shRNA
100
75
50
37
UCHL5
tubulin
Fig S3
D
K562
M - + shRNA
75
50
37
25
tubulin
HNRNPC
E
HTD114
M - + shRNA
75
50
37
25
tubulin
HNRNPC
F
K562
M - + shRNA
250
150
100
75
50
37
HNRNPL
tubulin
G
K562
M - + shRNA
150
100
75
50
37
HNRNPM
tubulin
H
HTD114
M - + shRNA
250
150
100
75
50
37
HNRNPM
tubulin
I
HTD114
M - + shRNA
100
75
50
37
25
HNRNPL
tubulin
J
K562
M - + shRNA
100
75
50
37
KHSRP
tubulin
K
HTD114
M - + shRNA
100
75
50
37
KHSRP
tubulin
L
HTD114
M - + shRNA
100
75
50
37
25
HNRNPUL1
tubulin
M
K562
M - + shRNA
100
50
HLTF
tubulin
N
K562
M - + shRNA
100
75
50
37
SAFB2
tubulin
O
K562
M - + shRNA
250
150
100
75
50
PTBP1
P
K562
M - + shRNA
75
50
HNRNPA1
tubulin

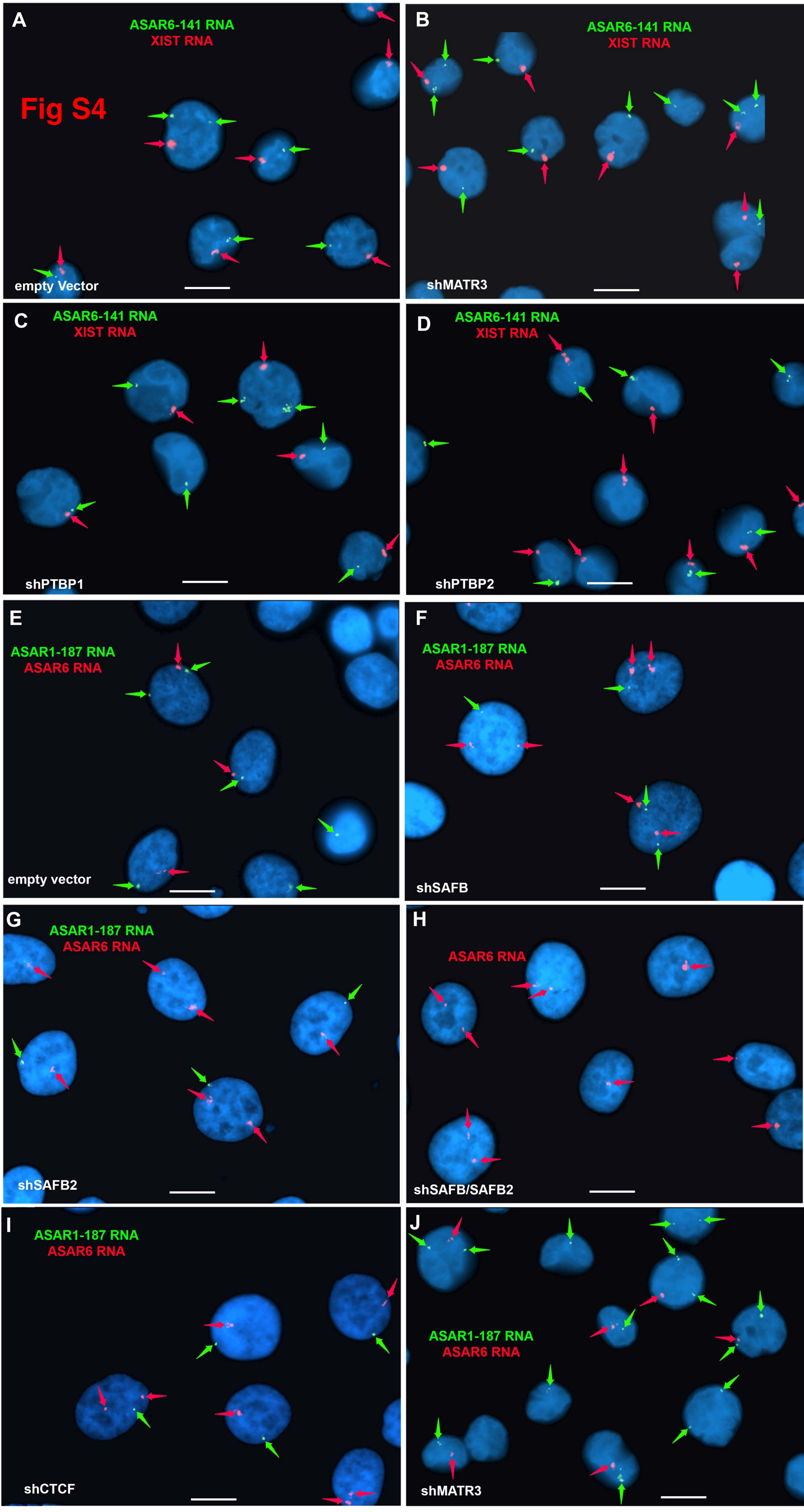
Fig S4
A
ASAR6-141 RNA
XIST RNA
empty Vector
B
ASAR6-141 RNA
XIST RNA
shMATR3
C
ASAR6-141 RNA
XIST RNA
shPTBP1
D
ASAR6-141 RNA
XIST RNA
shPTBP2
E
ASAR1-187 RNA
ASAR6 RNA
empty vector
F
ASAR1-187 RNA
ASAR6 RNA
shSAFB
G
ASAR1-187 RNA
ASAR6 RNA
shSAFB2
H
ASAR6 RNA
shSAFB/SAFB2
I
ASAR1-187 RNA
ASAR6 RNA
shCTCF
J
ASAR1-187 RNA
ASAR6 RNA
shMATR3

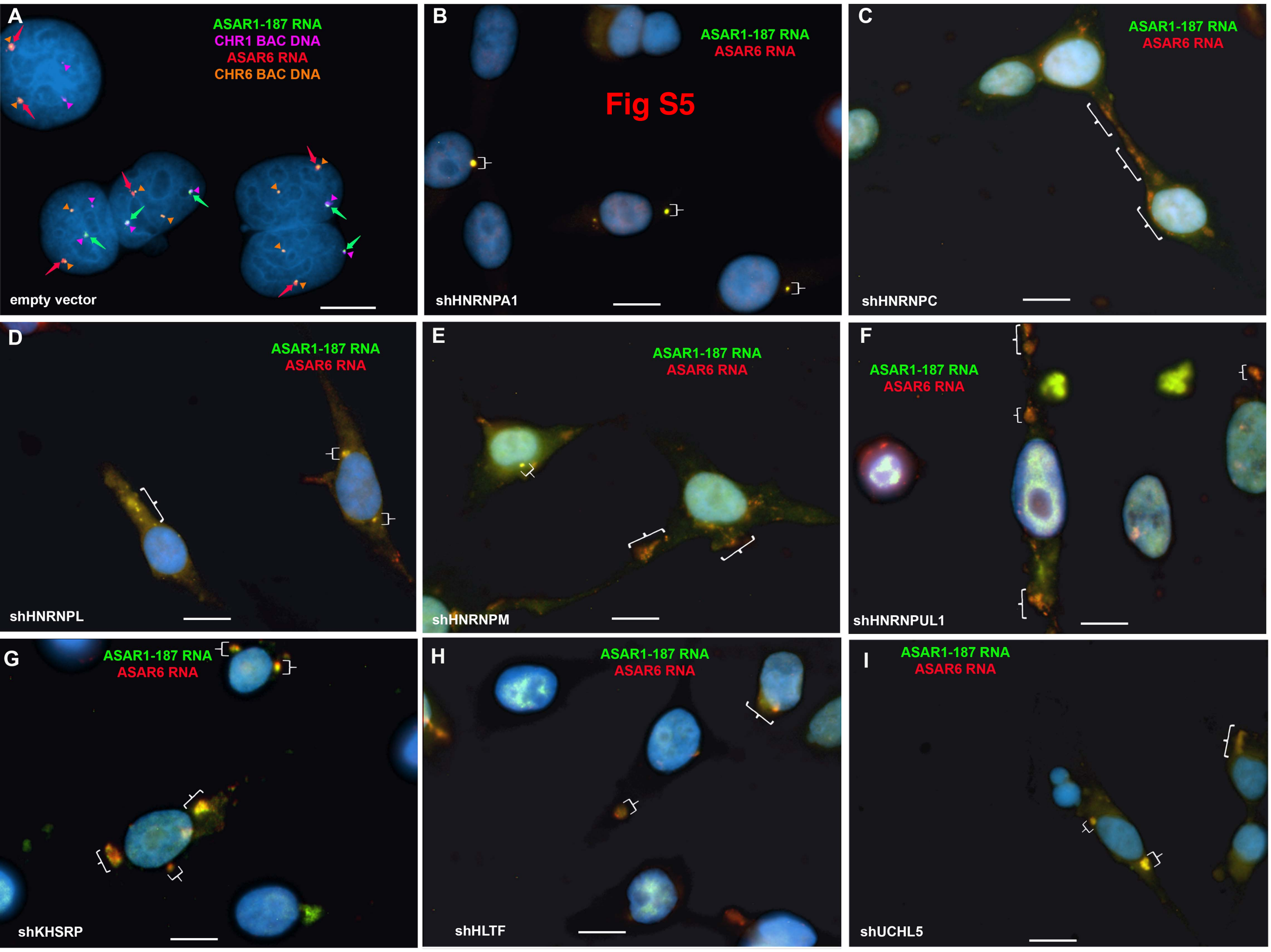
A
ASAR1-187 RNA
CHR1 BAC DNA
ASAR6 RNA
CHR6 BAC DNA
empty vector
B
ASAR1-187 RNA
ASAR6 RNA
Fig S5
shHNRNPA1
C
ASAR1-187 RNA
ASAR6 RNA
shHNRNPC
D
ASAR1-187 RNA
ASAR6 RNA
shHNRNPL
E
ASAR1-187 RNA
ASAR6 RNA
shHNRNPM
F
ASAR1-187 RNA
ASAR6 RNA
shHNRNPUL1
G
ASAR1-187 RNA
ASAR6 RNA
shKHSRP
H
ASAR1-187 RNA
ASAR6 RNA
shHLTF
I
ASAR1-187 RNA
ASAR6 RNA
shUCHL5

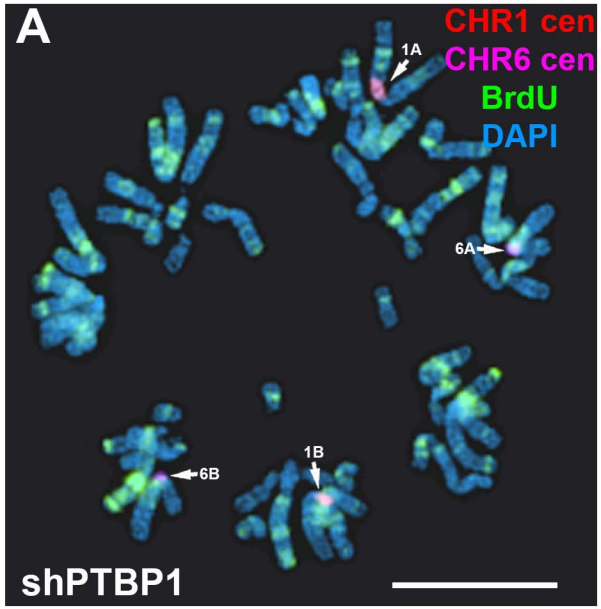

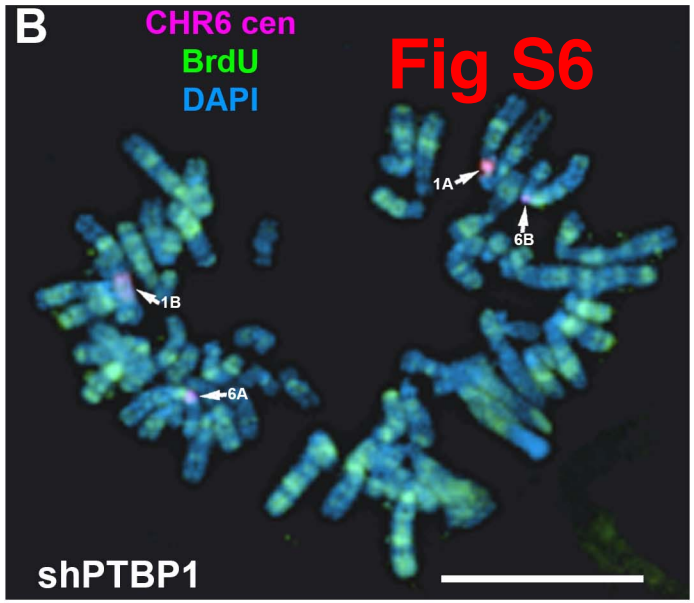

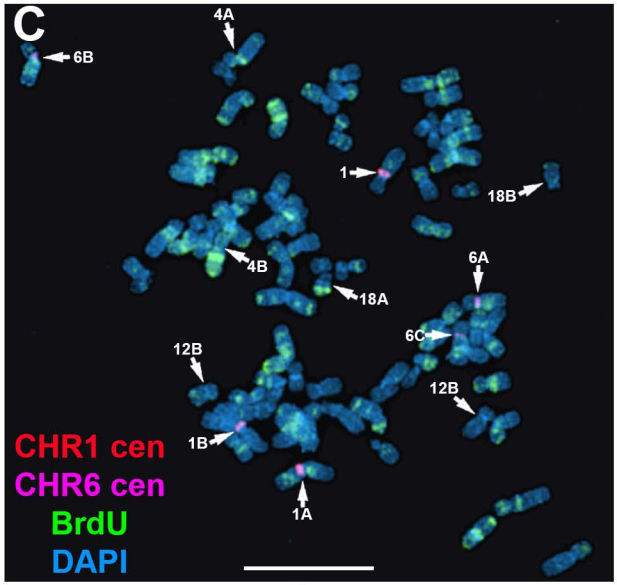

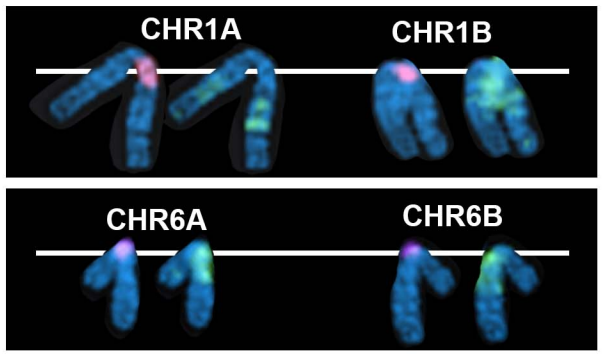

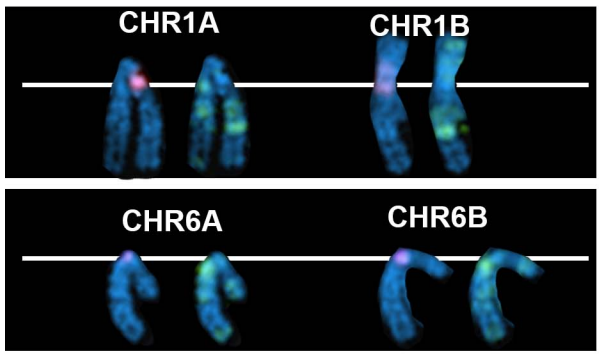

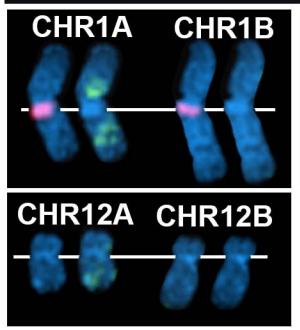

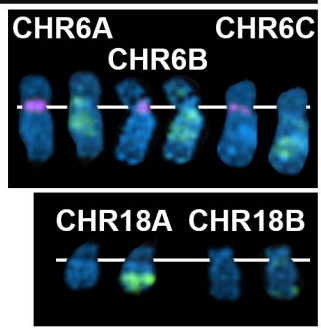

	Chromosome 1		
	1A	1B	
	Pixels	Pixels	ratio
DAPI	36176	42097	0.86
BrdU	4240	6700	1.6

	Chromosome 6		
	6A	6B	
	Pixels	Pixels	ratio
DAPI	27324	26316	1.0
BrdU	4664	4263	1.1

	Chromosome 1		
	1A	1B	
	Pixels	Pixels	ratio
DAPI	27404	38646	0.71
BrdU	3751	4240	0.89

	Chromosome 6		
	6A	6B	
	Pixels	Pixels	ratio
DAPI	23256	23865	0.98
BrdU	4718	4668	1.0

	Chromosome 1		
	1A	1B	
	Pixels	Pixels	ratio
DAPI	27885	35054	0.8
BrdU	4536	0	∞

	Chromosome 6					
	6A	6B	6C	ratios		
	Pixels	Pixels	Pixels	6A:6B	6A:6C	6B:6C
DAPI	20930	18767	24534	1.1	0.85	0.77
BrdU	4492	4064	3418	1.1	1.3	1.19

	Chromosome 12			Chromosome 18		
	12A	12B		18A	18B	
	Pixels	Pixels	ratio	Pixels	Pixels	ratio
DAPI	19700	14423	1.36	10354	11773	0.88
BrdU	2646	123	21.5	4713	245	19.2